Thin Solid Films 524 (2012) 1–19

Contents lists available at SciVerse ScienceDirect

Thin Solid Films

journal homepage: www.elsevier.com/locate/tsf

Critical review

Nanomaterials on flexible substrates to explore innovative functions: From energy harvesting to bio-integrated electronics

Ja Hoon Koo, Jungmok Seo, Taeyoon Lee *

Nanobio Device Laboratory, School of Electrical and Electronic Engineering, Yonsei University, 134 Shinchon-Dong, Seodaemun-Gu, Seoul 120-749, Republic of Korea

ARTICLE INFO

Article history:
Accepted 10 September 2012
Available online 9 October 2012

Keywords:
Flexible electronics
Elastomeric substrate
Stretchable electronics
Flexible substrate

ABSTRACT

Recent efforts in the semiconductor industry have focused on the realization of electronics with unusual form factors and functions which are not achievable using the current planar Si-based technology. Deposition of high-quality films or nanomaterials on low-temperature elastomeric substrates has been a technical challenge for flexible electronics. However, together with the development of new synthesis routes that enable the formation of robust thin films and nanomaterials on compliant substrates, including the dry transfer printing technique and fabrication of uniform nanogaps/nanowrinkles using the unique stretchable characteristics of elastomeric substrates, flexible electronics has emerged as a promising technology that can enrich our lives in a variety of ways. As examples, potential applications include skin-like smart prostheses, paper-like displays, disposable electronic noses, and hemispherically-shaped electronic eye cameras. Here, we review recent results demonstrating ingenious new functionalities using nanomaterials on flexible substrates, focusing on fabrication techniques, materials, operation mechanisms, and signal outputs.

Contents

1. Introduction

The concept of flexible electronics has been developed in earnest for little more than a decade in order to enable new applications which were not possible using conventional planar technology. In the early stages of development, polymer transistors were fabricated on pliable plastic or thin-glass substrates, primarily for electronic paper display devices [1,2], but the inherently poor electrical properties of the polymeric materials, compared with those of high-quality inorganic materials, were considered inadequate for other applications. In addition, the limitation posed by low-temperature processing, due to the use of elastomeric substrates, has made it difficult to deposit highly-refined active layers on such substrates, leading to degraded performance of fabricated devices. However, with the development

* Corresponding author.
E-mail address: taeyoon.lee@yonsei.ac.kr (T. Lee).

0040-6090/$ – see front matter © 2012 Elsevier B.V. All rights reserved.
http://dx.doi.org/10.1016/j.tsf.2012.10.001

of novel materials such as carbon-based structures [3], conducting polymers [4,5], metallic and ceramic composites [6–8], and nanomaterials [9,10], together with alternate cheap, fast, and facile deposition techniques such as roll-to-roll printing [1,11], transfer printing [12,13], and inkjet printing [14–17], high quality electronic structures encompassing diverse inorganic, organic, and composite materials can be formed on elastomeric substrates, thus opening up a new era in flexible electronics.

For the realization of flexible electronics, the most important consideration was the development of sustainable flexible systems which support high carrier mobility and good overall electrical performance, together with mechanical and environmental stability. The search for materials that can be used as active layers as well as substrates to overcome the constraints of mechanically inert systems still continues in parallel with defining the mechanics and underlying physics of these intrinsically heterogeneous structures. As a result, there are several review papers on the materials and mechanics of flexible electronics [18–26]. Not surprisingly, significant progress has been achieved both academically and industrially, and it is expected that within a few years, the first generation of commercial flexible devices will be demonstrated. The initial devices will likely be for display applications.

Recently, the scope of research has been extended to interdisciplinary fields including biotechnology and energy technology; the trend has evolved toward finding and developing a facile method of utilizing flexible systems to realize functions which are not possible with rigid systems. Combining rigid materials with elastomeric supports has resulted in the invention of novel devices, and hybrid structures are finding new possibilities and applications. The electronics can be deformed into curvilinear, cracked shapes while maintaining levels of electrical performance, device reliability, and integration that resemble those of high-quality wafer-based systems. In this review, we will discuss cutting-edge developments that utilize nanoscale thin films and low-dimensional materials on compliant substrates to exhibit innovative functions, and we will seek to understand the fundamentals of such systems. Additionally, insights into future strategies, routes to commercialization, new opportunities, and upcoming challenges for the realization of flexible integrated systems will be provided.

2. Energy scavenging systems

One of the areas rapidly gaining interest in flexible electronics is portable consumer devices, which are expected to soon evolve into wearable or implantable devices [27]. To turn these devices into “smart devices”, effort has been focused on improving computational ability and power management. While significant progress has been reported for enhancing computation speed; in the aspect of energy resources, there is plenty of room for improvement. Most of these devices use batteries as their power supply systems. To prolong the lifetime of the batteries, researchers seek new approaches to modify the materials and structures of the cathode, anode, and electrolyte [28,29]. There are still inherent limitations, however. Harvesting local energy sources can overcome such limitations or even eliminate them. Solar and thermoelectric modules have been investigated, but oftentimes these modules fail due to their strong dependency on environmental conditions [27]. As an alternate, research interests have lately been focused on harnessing electrical power from mechanical inputs, a common source much less affected by environmental conditions.

Mechanical strain is an abundant source of energy easily generated from everyday physical activities. It has been established by first generation devices [30,31] that substantial electricity can be obtained with optimized mechanical design and power management circuitry. For example, it was reported that up to 67 W of power can be generated by brisk human walk [32].

Piezoelectric materials serve as transducers to connect mechanical stress to electrical charge as a result of polarization. Applications in energy harvesting systems range from macro-systems such as electricity-generating speed bumps or walkways that can naturally collect power from transportation traffic or human beings, to small systems such as self-powered electronic switches and wireless doorbells without batteries. More recently, researchers are turning their focus to the realization of flexible piezoelectronic systems to facilitate bio-mechanical energy scavenging based upon nanomaterials. Sections 2.1 and 2.2 introduce general aspects of piezoelectrics and present results in material development and device structures. Device operation mechanisms and output performance will also be discussed.

2.1. Piezoelectricity

The direct piezoelectric effect is the conversion of mechanical stress into electrical charge, while the inverse effect is the transformation of an applied electrical field into mechanical stress. Direct piezoelectricity is caused by a reconfiguration of dipole-inducing ions on crystal lattice sites with asymmetric charge distributions due to the influence of an external stress. This is illustrated using the piezoelectric compound ZnO (Fig. 1(a)) in Fig. 1(b). ZnO has the wurtzite structure in which alternating planes along the *c*-axis are composed of tetrahedrally-coordinated Zn^{2+} and O^{2-}. When an external strain is applied, the cation and anion centers of charge, which coincide with each other in the absence of strain, are separated, leading to the formation of an electric dipole. This property can be utilized to generate electricity.

The mechanical and electrical behavior of direct piezoelectric materials can be modeled using the linear constitutive equation [33,34],

$$S_i = S_{ij}^E T_j + d_{ki} E_k, \tag{1}$$

in which S and T are the strain and stress tensors induced by the mechanical and electrical effects, respectively; s^E is the elastic compliance matrix evaluated at a constant electric field; d is a tensor of piezoelectric coefficients; E is the electric field vector; and the subscripts i, j, and k represent the three orthogonal spatial directions. Here, the piezoelectric coefficient charge d, the polarization generated per unit mechanical stress applied to a piezoelectric material, is the most critical factor affecting the energy conversion efficiency. However, careful consideration must be given when choosing an appropriate piezoelectric material according to specific applications rather than simply selecting materials with larger values of d since the latter advantage is frequently offset by other factors such as flexibility, cycling longevity, cost, fabrication convenience, and form factor. In addition, the dimension and size of the piezoelectric materials should be considered.

Table 1 lists the most frequently used piezoelectric thin films and nanomaterials together with their properties. It can be seen that even for the same material, piezoelectric properties can be substantially different depending upon structure. For example, the piezoelectric charge of bulk ZnO, 9.93 pC N^{-1}, increases to 26.7 pC $N^{-1}$when fabricated in nanobelt form [35].

Details of the piezoelectric effect, including the underlying physics and analytical methods used to model piezoelectric materials, are readily available in the literature: journal papers, conference proceedings, and books [43–50]. The primary topic here is flexible energy scavenging devices that can endure high levels of strain in order to be applicable in wearable or implantable systems. In the following section, we discuss recent achievements demonstrating practical routes to realizing wearable energy scavenging devices: the materials and structures adopted, their interaction with elastomeric substrates, and fabrication methods.

2.2. Piezoelectric nanogenerators with unusual form factors and structures

Recent research interests have focused on the integration of high-performance nanoscale piezoelectric energy harvesting devices fabricated with unusual form factors on unconventional bendable substrates [51–54]. The major technical concern lies with the stretchability of the

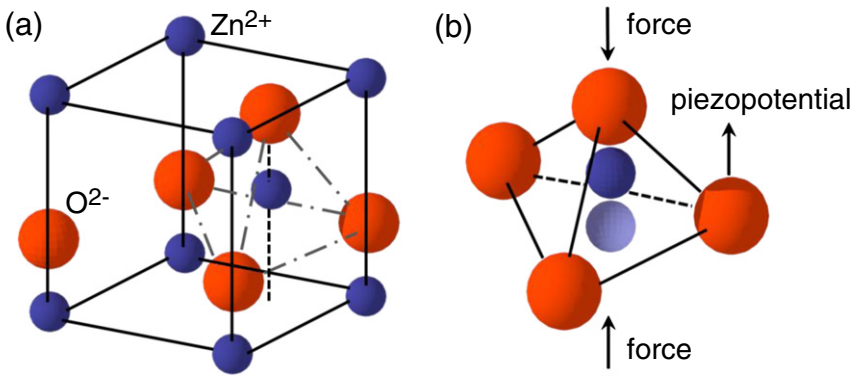

Fig. 1. (a) Model structure of wurtzite-structure ZnO. (b) Generation of a piezoelectrical potential in a ZnO crystal under applied stress.

piezoelectric materials, since the strain levels required to achieve practical wearable devices often exceed the fracture limits of piezoelectric materials. It has been reported that an inherently flexible and stretchable polymeric polyvinylidine fluoride (PVDF), which is one of the most durable piezoelectric materials under bending, can accommodate a maximum strain of 2%, or slightly higher, when fabricated as nanofibers [55]. However, PVDF has relatively weak electrochemical coupling characteristics with a piezoelectric coefficient near −25 pC N^{-1}. Materials with high piezoelectric coefficients can be found among inorganic ceramics, but most are mechanically brittle. For example, the piezoelectric coefficient of lead zirconate titanate (PZT) is nearly 10 times that of PVDF, but its fracture limit is only 0.2% tensile strain with an elastic modulus of 50–100 GPa [56]. Although one-dimensional structures of these ceramic piezoelectrical materials possess higher flexibility than their bulk counterparts, many reports show that nanoribbons of PZT [43,57,58], barium titanate ($BaTiO_3$) [59,60], or ZnO [40,41] printed onto elastomeric substrates are susceptible to damage under repeated stretching and folding.

Much effort has been expended in developing a novel route to develop materials that exhibit high piezoelectric performance while maintaining mechanical integrity under stretching and bending operations. For example, Qi et al. [61] enhanced the flexibility of PZT ribbons by transforming them into buckled forms, using prestrained polydimethylsiloxane (PDMS) substrates, and peeling the ribbons off (Fig. 2(a)). The ribbons, which buckled upon stress relaxation, can tolerate substantially larger compressive and tensile strains via changes in the amplitudes of the buckled PZT nanoribbons. Whereas the maximum tensile strain that bulk PZT can tolerate is approximately 0.2%, the tolerance greatly improves to nearly 8% in buckled PZT nanoribbons. The upper and lower scanning electron microscope (SEM) images in Fig. 2(b) show stretching of buckled PZT ribbons from 0 to 8.1% tensile strain with no cracks or other fractures. Fig. 2(c) is a plot of the electrical response, i.e. energy conversion, due to stretching and releasing the buckled PZT ribbons using the experimental setup illustrated in Fig. 2(d). The current was measured for a device consisting of 10 ribbons under periodic stretch (8% strain) and release with a frequency of 0.6 Hz. The buckled ribbons demonstrated an enhanced current density of ~2.5 μA/mm^2, which compares favorably to the peak current densities measured with PZT nanowire-based devices, ~0.1 μA/mm^2 [54,62]. These results show that heterogeneous platforms of rigid nanostructures on elastomeric substrates can be applicable to wearable or even implantable energy-harvesting devices.

Lee et al. [63] adopted hybrid piezoelectric materials to construct a nanodevice that generates electricity from mechanical activity at very low frequencies, below 1 Hz. A conducting fiber was surrounded with arrays of ZnO nanowires (NWs) and then covered with PVDF polymer as shown schematically in Fig. 3(a). The ZnO NWs, synthesized using the hydrothermal method [64–66], serve as the core piezoelectric potential generator and an additive to maximize the surface-contact area. The surrounding PDVF polymer also acts as a piezoelectric potential generator, but its major contribution is to increase the overall durability of the hybrid structure under deformation. Piezoelectricity is generated from the two components upon bending or elongating the hybrid fiber and, as a proof-of-concept, the performance of the hybrid fiber was tested by attaching it to a human arm (Fig. 3(b)). In accordance with the folding and opening action of the arm, the hybrid-fiber nanogenerator exhibits voltage and current-density outputs of ~0.1 V and 10 nA cm^{-2} (Fig. 3(c)), indicating that fiber nanogenerators are promising structures as energy-harvesting components based upon low-frequency mechanical activities of humans and animals.

Table 1
Summary of piezoelectric materials and their properties.

Structure	Material	Piezoelectric charge d_{33} [pC N^{-1}]	Relative dielectric constant $(\varepsilon/\varepsilon_0)^*$
	Lead zirconate titanate (PZT) [36]	60 to 130	300 to 1300
	$BaTiO_3$[34]	191	1700
Thin film	ZnO[34]	5.9	10.9
	Polymeric polyvinylidine fluoride (PVDF)[34]	−33	13
	AlN[34]	3.9	10.5
Nanomaterial	PZT-fiber [37,38]	54.2 to 460	300 to 500
	PZT-PDVF composite [39]	13 to 25	80
	PZT-polymer composite [40]	1 to 20	19 to 47
	ZnO[32] [41,42] (nanowires, nanorods, etc.)	0.4 to 26.7	2.7 to 7.8

*ε: complex frequency-dependent absolute permittivity of the material. ε_0: vacuum perimittivity.

3. Unconventional sensing systems

The building blocks of modern sensing systems are composed of electronic and optoelectronic semiconductor components which are typically attached to mechanically inflexible printed circuit boards (PCBs). Even though these systems can be fabricated on polymer-based elastomeric PCBs that offer a small bending radius in the range of few centimeters along a single axis, they are easily fractured from fatigue strain and/or excessive bending [67]. Devices which are highly flexible, conformal to rugged morphologies, and mechanically resistive to fatigue strain would greatly expand the applicability of future electronics. Possible applications include convenient, portable (or wearable) electronic sensors that

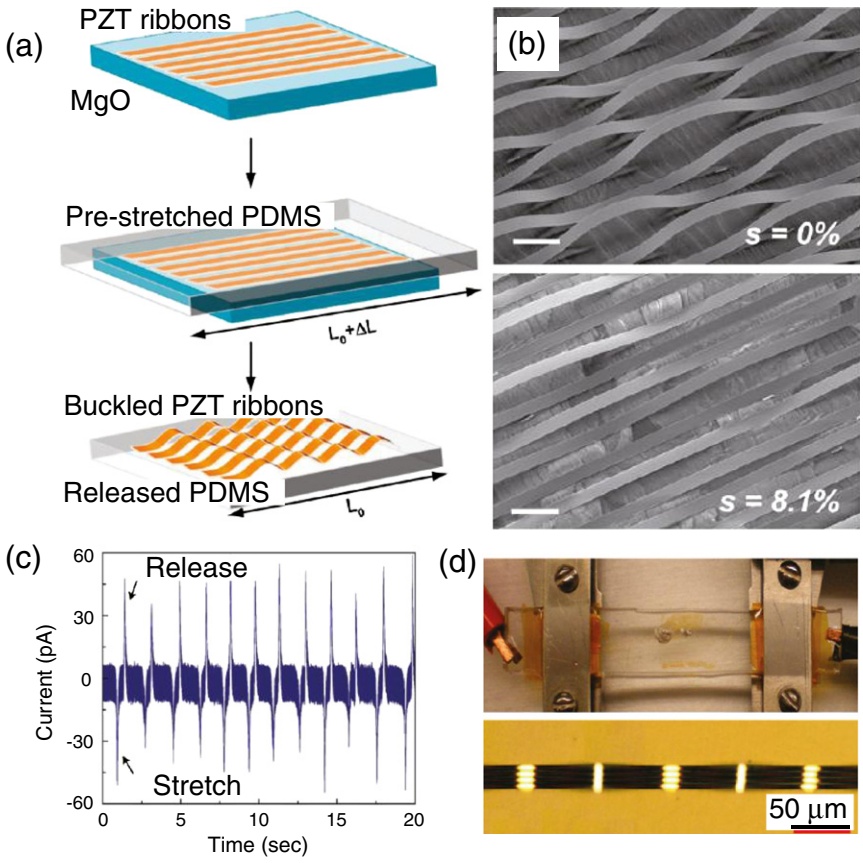

Fig. 2. (a) Schematic illustration of forming wavy/buckled piezoelectric PZT ribbons. PZT ribbons were firstly patterned on a MgO substrate; then, they were transferred onto a pre-strained PDMS and peeled off. The wavy/buckled structures were formed upon strain relaxation. (b) SEM image of transfer-printed PZT ribbons with the applied strain released; top, strain = 0% and bottom, strain = 8.1%. The scale bars indicate 20 μm. (c) Electrical response of the fabricated PZT ribbons during periodic stretch and release. (d) Digital image of the experimental apparatus. Top: photograph of the stretching stage and the device mounted on it; bottom: optical micrograph of buckled PZT ribbons with silver-paint contacts.

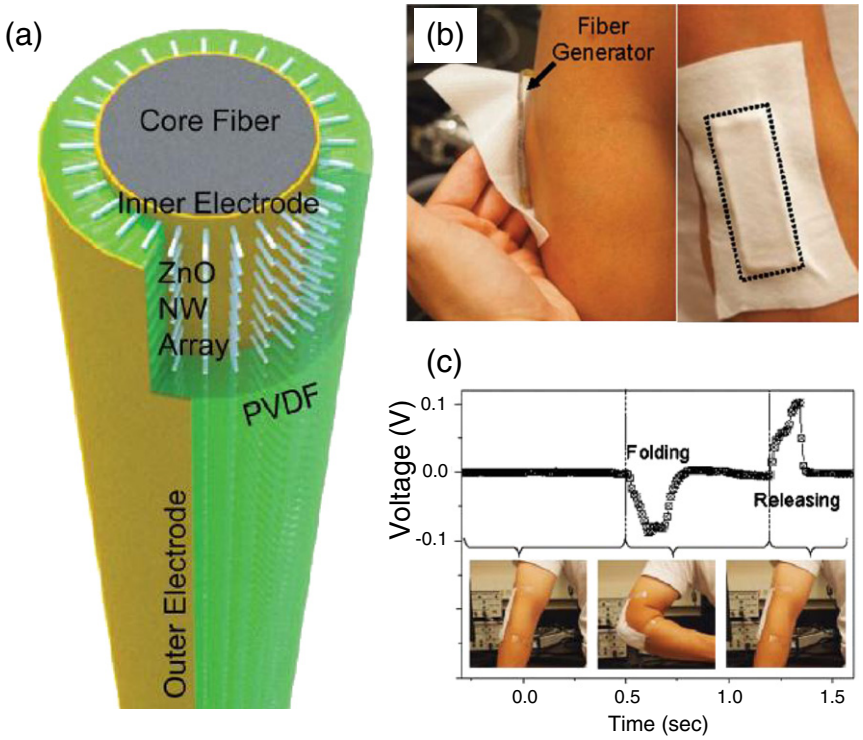

Fig. 3. (a) Schematic 3D diagram of a hybrid-fiber device consisting of a ZnO NW array wrapped around a PVDF polymer. (b) Digital image of a nanogenerator attached to a human elbow. (c) Electrical response of the attached nanogenerator to motions of the arm.

can detect low levels of toxic compounds, pollutants, and other hazardous substances, and an "electronic skin" which can detect tactile information through pressure changes. In this section, features of flexible sensing devices consisting of nanomaterials on elastomeric substrates will be discussed.

3.1. Chemical sensors using flexible systems

The use of semiconducting nanomaterials, particularly those with high surface-to-volume ratios such as NWs and nanorods, can be beneficial for achieving higher chemical sensitivity [68–78]. During the past few decades, sensors based on Si nanomaterials, various oxide nanomaterials, and carbon-based nanomaterials have been extensively researched owing to their applicability in various chemical and biological sensing systems. Table 2 summarizes the types of analytes that have been detected using these materials.

Recently, the focus has been to implement these materials on biocompatible, flexible substrates with the hope of yielding breakthroughs in implantable or wearable monitoring systems. Synthesis of high-quality semiconducting materials on thermally-sensitive compliant substrates has been difficult. Instead, the dry-transfer technique is used to relocate the as-deposited high-quality semiconductor materials from the host substrates to plastic substrates using PDMS, poly(methyl methacrylate) (PMMA), or other soluble glues [123–125].

McAlpine et al. successfully used the dry transfer technique to integrate single-crystalline Si nanowire arrays onto plastic substrates in order to fabricate a flexible chemical sensor with high sensitivity and low power and heat dissipation [126]. The highly-ordered Si NW arrays were fabricated from a doped silicon-on-insulator wafer; the Si NWs were defined through anisotropic etching using a protective cleaved GaAs/$Al_xGa_{1-x}As$ superlattice membrane mask. Etching the buried oxide in concentrated hydrofluoric acid (HF) released the NWs without misalignment of the NW arrays, and a slab of PDMS was used to transfer-print the arrays onto a plastic substrate. The diameter of a single NW was approximately 18 nm, and the width of the transferred NW array was about 16 μm with an average pitch of nearly 41 nm. Fig. 4(a) is an SEM image of a Si NW array and the actual sensor (inset), where each device is contacted by two vertically-oriented electrodes that extend to larger pads.

Upon exposure to nitrogen dioxide gas (NO_2), the current flow greatly increases due to the strong electron-acceptor characteristic of NO_2, which is equivalent to injecting hole carriers into the p-type Si NWs. Fig. 4(b) shows electrical responses of the NW sensors upon NO_2 exposure up to 200 parts per billion (ppb). Although laborious efforts were required to prepare the Si NW arrays, in addition to the transfer process, the work clearly demonstrates an effective method to fabricate flexible chemical sensors with exquisite sensitivity. The authors have excellent controllability of the alignment of the nano-structures.

Table 2
Summary of materials used in chemical sensing devices and analytes.

Materials	Analyte	References
Si	NO_2, NH_3, H_2, CO, H_2O, ethanol, SO_2	[79–81]
Carbon nanotube	NO_2, NH_3, H_2, CH_4, CO, SO_2, H_2S, O_2, NO, ethanol	[82–85]
Graphene	NO_2, NH_3, H_2, CO, H_2O, ethanol	[86,87]
Graphene oxide	NO_2, NH_3, H_2, CO, H_2O	[78,88,89]
ZnO	NO_2, NH_3, H_2, CH_4, CO, H_2S, O_2, NO, H_2O, ethanol	[90,91]
SnO_2	H_2, CH_4, CO, SO_2, O_2, H_2O, ethanol, C_2H_2	[92–95]
InO_x	NO_2, CH_4, CO, ethanol, O_3	[96,97]
WO_3	NO_2, NH_3, H_2, CH_4, CO, SO_2, H_2S, O_2, NO, Benzene, ethanol, O_3, Cl_2	[98–102]
MgO	NO_2, SO_2, O_2	[103]
TiO_2	NO_2, NH_3, CO, SO_2, O_2	[104–113]
ZrO_2	NO_2, NH_3, CO, SO_2, H_2S, O_2, ethanol	[114–118]
Pd	H_2	[119–122]

Despite the success of McAlpine et al.'s work, the transfer of a highly ordered array of nanomaterials with desired spatial alignment is challenging. The transferred nanomaterials may lose their original shapes or be damaged during the transfer process, leading to severe degradation in device performance and device yield. The transfer of more dense composites would lead to less distortion of their original forms owing to the stronger interaction among the nanomaterials.

Jeong et al.'s report [127] describes a highly sensitive flexible chemical sensor based on carbon nanotubes (CNTs)/reduced-graphene hybrid films, in which the hybrid composite films were prepared by solution casting reduced graphene films on SiO_2 substrates followed by the growth of CNTs using plasma-enhanced chemical vapor deposition (PECVD) directly on top of the reduced graphene film. The as-prepared CNT/reduced-graphene nanocomposites were then dry transferred onto Au/polyimide flexible substrates. Fig. 5(a) is a schematic illustration showing the structure of the fabricated flexible device, and Fig. 5(b) is an image of the device under bending. The flexible sensor is highly sensitive to NO_2 gas at concentrations in the range 0.5 to 10 parts per million (ppm) (Fig. 5(c)), and functions well over a substantial temperature range from room temperature to 350 °C (Fig. 5(d)).

In a report by Yi et al. [128], a hybrid structure consisting of a graphene layer over the top of vertically-aligned ZnO nanorods was used to detect ethanol gas (CH_3CH_2OH). Here, the vertically-aligned ZnO nanorods and graphene coated with thin metal layers were separately prepared and brought together using a modified dry-transfer

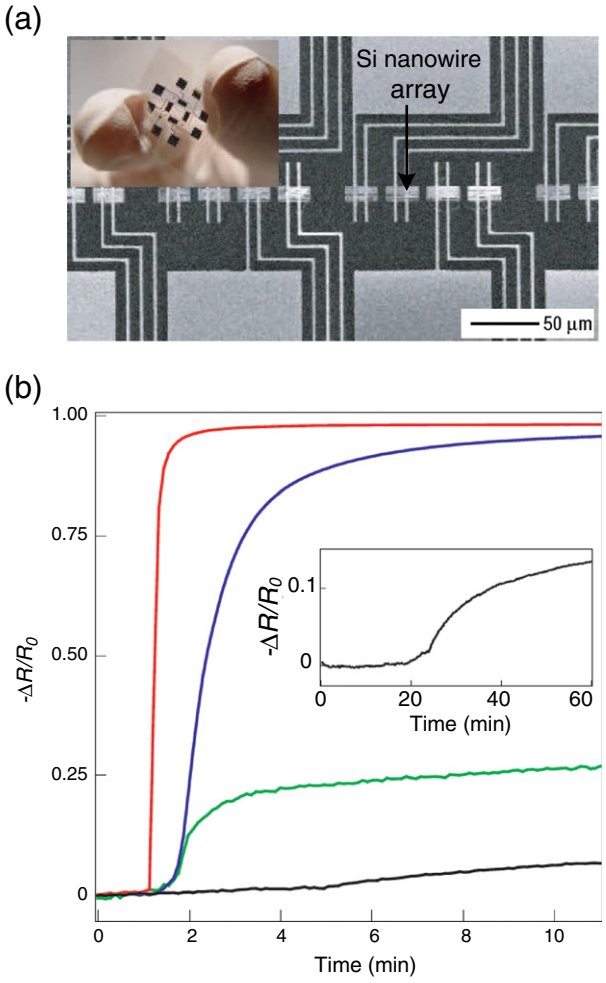

Fig. 4. (a) SEM, and (inset) digital photographic image, of a fabricated flexible nanowire-on-plastic gas sensor. (b) Electrical response with respect to time to various concentrations of NO_2 in N_2; the inset shows the extended response of the sensor to 20 ppb NO_2.

technique. Accordingly, the resulting ZnO-nanorods/graphene hybrid architecture retains appropriately designed distances between the monolithic nanorods, allowing for facile and rapid gas transport.

Fig. 6(a) and (b) shows an illustration and cross-sectional SEM images of the ZnO-nanorods/graphene hybrid structure. Despite the variance of the height and vertical alignment of the nanorods which led to imperfect contact between the ZnO nanorods and graphene, the adhesion between the two was sufficiently reliable that approximately half of the ZnO nanorod tips form robust bonds to the graphene by van der Waals forces (Fig. 6(b)). Fig. 6(c) plots conductance changes as a function of ethanol gas exposures from 10 to 50 ppm. The electrical conductivity of the ZnO nanorods increases when exposed to a reducing gas such as ethanol. This is attributed to the substitution of the surface-bound oxygen and consequent injection of electrons into the ZnO crystals. The sensitivity of the sensor, which can be defined as the ratio of the resistance recorded in the presence of ethanol gas to that of air, is approximately 90 for 50 ppm ethanol gas.

The challenge of nanostructure assembly was addressed differently, and more simply, in the work of Lee et al. using a stretchable substrate [129]. Notably, their method was lithographic-free and transfer-free, but instead makes use of the stretchability of the elastomeric substrate to fabricate uniformly-distributed nanostructures with excellent controllability. By applying a lateral tensile strain on a Pd thin film deposited on a flexible PDMS substrate, uniform and linear nano-sized gaps, whose size could be controlled to 300 nm at a tensile strain of 25%, were generated in the Pd film over a large area. Fig. 7(a) illustrates the mechanism of nanogap formation in the Pd thin film; stretching the Pd film on PDMS along a lateral direction creates linear cracks in directions perpendicular to the Pd film elongation. The widths of the cracks are approximately 2 μm and the cracks are separated by ~15 μm. Upon the relaxation of the tensile strain, the cracks are reconnected through contraction, but they were converted into nanogaps after being exposed to hydrogen gas (H_2). This is attributed to the unique property of volumetric change in Pd by the adsorption and removal of H atoms. The nanogaps in Pd thin films are used to detect H_2.

Fig. 7(b) plots the real-time electrical response of a flexible Pd nanogap-based sensor to 4% H_2 at room temperature, showing a clear periodic pulse train while alternating the ambient between N_2 and H_2. The morphology change of the Pd thin film during the alternating environment is illustrated to the right of Fig. 7(b). At the initial stage (i), the cracks formed in the Pd layer hinder the flow of current; when exposed to H_2 (ii), the current increases dramatically due to the volumetric expansion of the Pd, leading to a reduction in the gap and reestablishment of the current path. When the ambient is changed to N_2 (iii), desorption of H_2 atoms leads to volumetric shrinkage of the Pd film, thereby opening up the nanogaps that block the flow of current. The lithographic-free approach described in Lee et al.'s report enables facile formation of highly-aligned nanoscale structures over large areas with excellent uniformity. This method is not restricted to Pd for sensing H_2, but can be applied to other metals to create nanogaps for sensing specific chemicals with nearly perfectly reversible on/off behavior.

3.2. Pressure sensors using flexible systems

Strain sensors which monitor force, pressure, shape, and strain are widely researched for future applications [130,131]. For example, artificial electronic skin capable of recognizing the environment through tactile information can bring enormous advancement in the areas of robotics and prosthetic applications. The realization of such electronic skin requires pressure-sensitive devices that support sustainable sensitivity in low-pressure regimes and fabrication on a thin, yet large flexible substrate. Despite recent development in flexible electronics in general, little progress has been achieved in the field of pressure sensing compared to areas such as chemical or image sensing [137,138]. This is attributed to the lack of adequate materials for fabricating a flexible switching matrix, which cannot be done using current silicon-based technology. Although organic field-effect transistors (OFETs) have been the focus as the switching matrix in pressure sensors due to their inherently flexible nature and cost-effectiveness for large-scale integration, their sensitivity and responsivity are insufficient in the low-pressure regime (<10 kPa, comparable to a gentle touch) and this is considered to be the major obstacle in their utilization as pressure sensors.

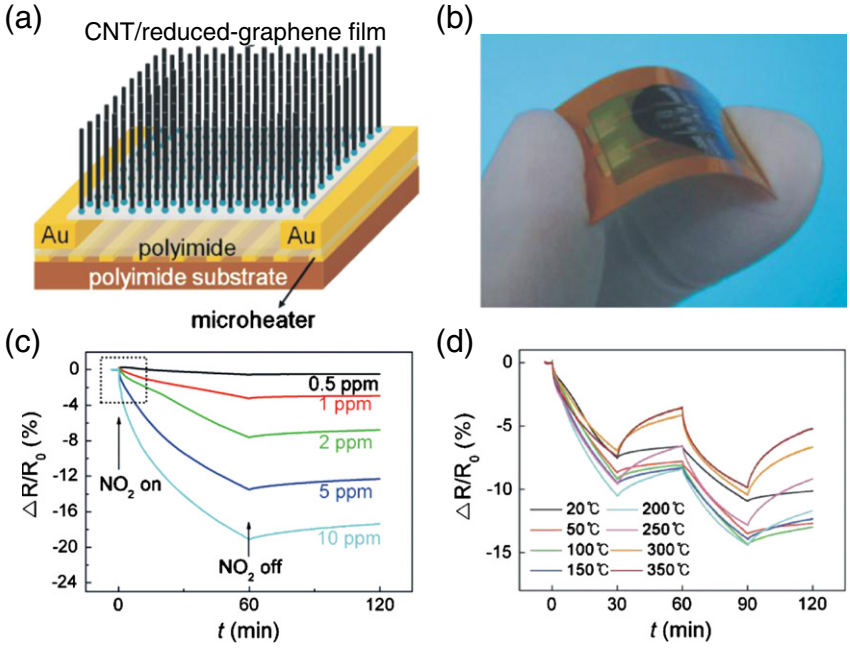

Fig. 5. (a) Schematic illustration of a device consisting of CNTs/reduced-graphene film on a flexible polyimide substrate. (b) Digital photographic image of the fabricated flexible sensor under bent condition. (c) Electrical response to various concentrations of NO_2 with respect to time. (d) Electrical response of a flexible CNT/reduced-graphene sensor to 5 ppm NO_2 at various temperatures.

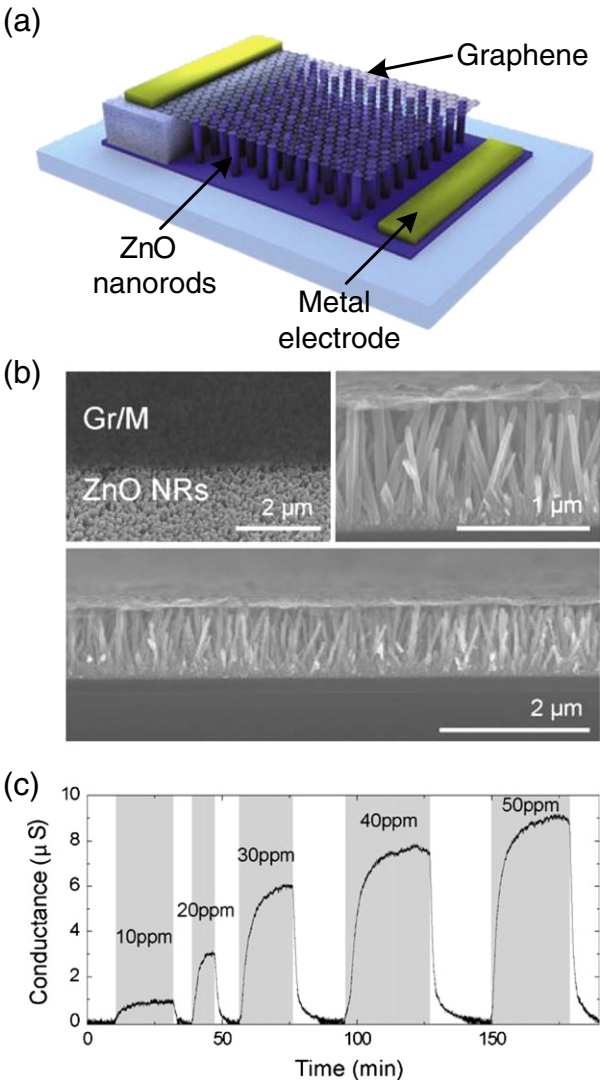

Fig. 6. (a) Schematic illustration of a ZnO nanorods/graphene hybrid structure. (b) SEM images of the hybrid structure. (c) Electrical response of the flexible ZnO nanorod/graphene sensor to various concentrations of ethanol.

In a recent report by Mannsfeld et al. [132], the sensitivity and responsivity of OFETs were greatly enhanced by adopting a regularly-structured thin compressive rubber dielectric layer, which affects the dielectric capacitance, and hence the output current of the OFET devices. This work was unique in that the elastomer PDMS was not used as a durable backplane to provide flexibility in the fabricated device, but rather used as a nanostructured dielectric thin layer to maximize the sensitivity of the fabricated device while maintaining its flexible function.

Fig. 8(a) is a schematic illustration of a pressure-sensing OFET, consisting of thin rubrene single crystals and a PDMS dielectric layer with regular and uniform nanostructures (2–3% pitch fidelity). The PDMS film was designed to be nanostructured in order to prevent, via regularly positioned voids, visco-elastic creep. In a planar structure, the PDMS film would not be able to return to its original structure after the application of external pressure due to irreversible entanglement of polymer chains.

The enhanced restoring force obtained by adopting a nanoengineered PDMS dielectric layer led to unprecedented pressure sensitivities as can be seen in Fig. 8(b). A clear capacitance change was observed upon placing and removing a bluebottle fly (20 mg), comparable to applying a pressure of only 3 Pa. In addition, the response and relaxation times of the fabricated sensor were in the millisecond range, more than 100 times faster than those previously reported using similar materials [133,134]. This is attributed to the use of thin (<10 μm) nanostructured PDMS films which minimize the parasitic capacitance in the readout circuitry, thereby providing a good signal-to-noise ratio.

As proof of concept, a capacitive matrix-type pressure sensor that is flexible and "all-plastic," except the metal electrodes, has been fabricated using a nanostructured PDMS film sandwiched between polyethylene terephthalate layers. The actual device and the pressure response to the tripod are shown in Fig. 8(c). The rapid response time, and hence rapid collection of pressure data due to the use of a nanostructured dielectric layer, can be applicable to the development of highly intuitive electronic-skin applications.

Instead of using all organic materials, Takei et al. [135] assembled Ge/Si core/shell NW arrays on a polyimide substrate using contact-printing and created a NW-array field-effect transistor that detects pressure changes in the range up to 15 kPa. The aim was to achieve higher charge carrier mobilities and lower operating voltages with the use of inorganic crystalline semiconductors. The process scheme for the sensor device is shown in Fig. 9(a), in which a laminated pressure-sensitive rubber (PSR) is used as the sensing element [136,137].

The use of highly-aligned NW arrays led to a high on-current of approximately 1 mA at $V_{DS} = 3$ V, with a peak field-effect mobility of ~20 $cm^2\ V^{-1}\ s^{-1}$, measured prior to PSR deposition. Following PSR integration, the NW-array FETs exhibited high sensitivity to

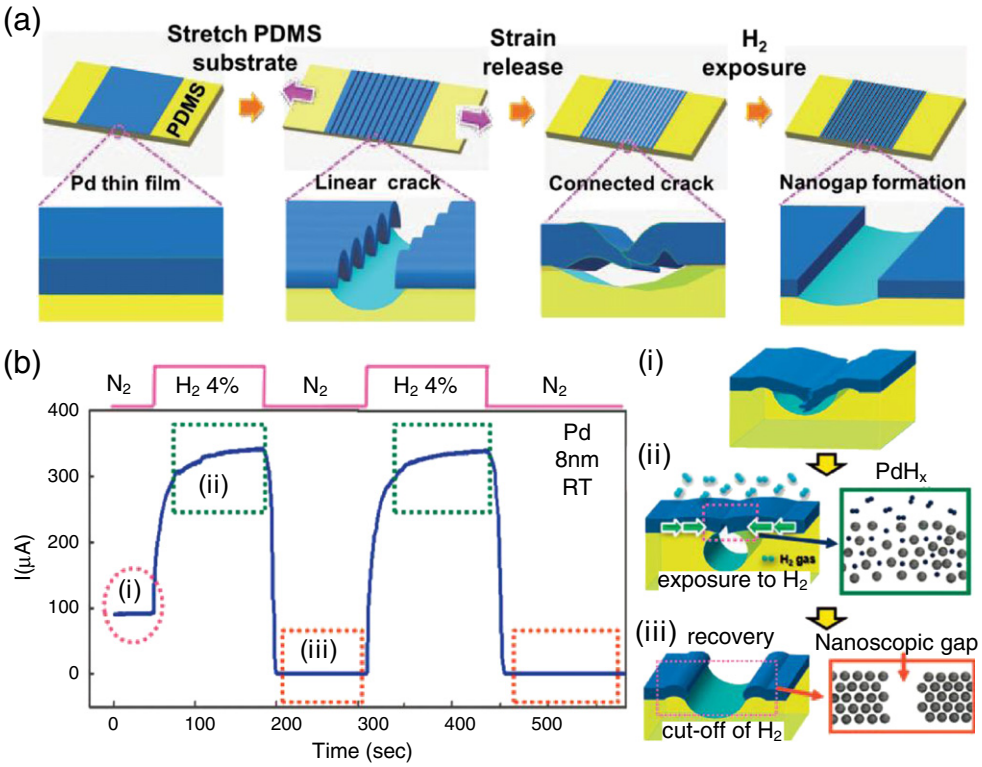

Fig. 7. (a) Schematic illustration of nanogap formation, due to applying and releasing tensile strain in a Pd thin film deposited on a PDMS substrate, followed by exposure to H_2. (b) Real-time electrical response of a nanogap-based Pd film sensor to 4% H_2 exposure at room temperature. The regions labeled (i) to (iii) in the plot correspond to the illustrations on the right.

applied normal pressures ranging from 2.2 to 14.4 kPa (Fig. 9(b)). The sensitivity gain originated from the conductance change, due to the PSR, upon application of pressure. Specifically, the average separation between conductive carbon nanoparticles inside the PSR is significantly shortened in the presence of an applied pressure, leading to noticeable conductance changes immediately. The on-state conductance of the NW-array FETs showed an exponential pressure dependency for $P \leq 2$ kPa, beyond which the dependence is linear up to the maximum applied pressure of ~15 kPa (Fig. 9(c)). Time-resolved measurements and mechanical flexibility tests showed that the devices are responsive without significant signal degradation up to 5 Hz, and mechanically stable with minimal performance degradation even after 2000 bending cycles (radius of curvature of 2.5 mm). As a practical application, a 19×18 pixel array e-skin was fabricated with a physical size of 7×7 cm^2 and a slab of PDMS molded as the letter *C* placed on top of the sensor array. The output conductance for each individual pixel was measured upon the application of a normal pressure of ~15 kPa, and plotted as a two-dimensional intensity map as shown in Fig. 9(d). The yield of functional active pixels was as high as 84% with the defective pixels caused primarily by the failure of process integration steps. Thus, much higher yield should be achievable with more refined processes.

Using aligned single-walled carbon nanotube (SWCNT) thin films, Yamada et al. [138] demonstrated a new type of stretchable strain sensor with remarkable features such as high endurance to strain up to 280%, high durability, a fast response time of 14 ms, and low creep of 3.0% at 100% strain. Fig. 10(a) schematically illustrates the key processes in fabricating and operating a SWCNT film strain sensor. The primary idea here is to place SWCNT thin films side-by-side with uniform overlaps (1 mm in the report), and flatten them through wetting with isopropyl, ensuring a strong van der Waals contact that can endure extreme mechanical deformations. Fig. 10(b) depicts sequential images of the SWCNT film from initial loading, up to a strain level of 100% where the strain was applied along the direction indicated by a white dotted arrow in the left image.

Fig. 10(c) plots the resistance changes of the SWCNT film strain sensor in response to mechanical strain up to 100%. The resistance change can be ascribed to the formation of gaps and islands in the SWCNT film, as illustrated in Fig. 10(d). At the onset of strain exertion, irreversible gaps and islands (indicated in Fig. 10(b)) were formed, and the film fractured. The number of gaps, their widths, and the number of islands increased with further strain. The created gaps and islands remained after the unloading of applied stress, and neither new gaps nor islands were created during the subsequent phases. Instead, all of the strain was absorbed by a reversible opening and closing of the gaps. The reversible fracturing of the SWCNT film explains the extreme level of stretchability, which also allows exceptional durability with little degradation, as demonstrated by the 10,000 cycle durability test (not shown here). The potential of SWCNT films in wearable devices was demonstrated by fabricating a bendable strain sensor and attaching it to a human knee to measure electrical responses according to different human activities. Fig. 10(e) presents the relative change in resistance to different knee motions; different patterns of resistance change were related to specific motions, which infer that the activity patterns of human motions and exercises can be recognized using the SWCNT film strain sensor.

4. Flexible bioelectronics

The area that is expected to benefit most from the development of flexible devices is biomedical science, since biology is naturally curved, elastic, and soft. As examples, diagnostic and surgical apparatus that genuinely integrate with the human body can provide enhanced therapeutic capabilities, and implantable electronic energy harvesters that can provide sufficient and sustainable power for artificial internal organs or other electronic medical implants will eliminate the necessity to replace them. Such examples are the mere “tip of an iceberg”, and together with nanotechnology, the actualization of advanced functions which allow new means of health

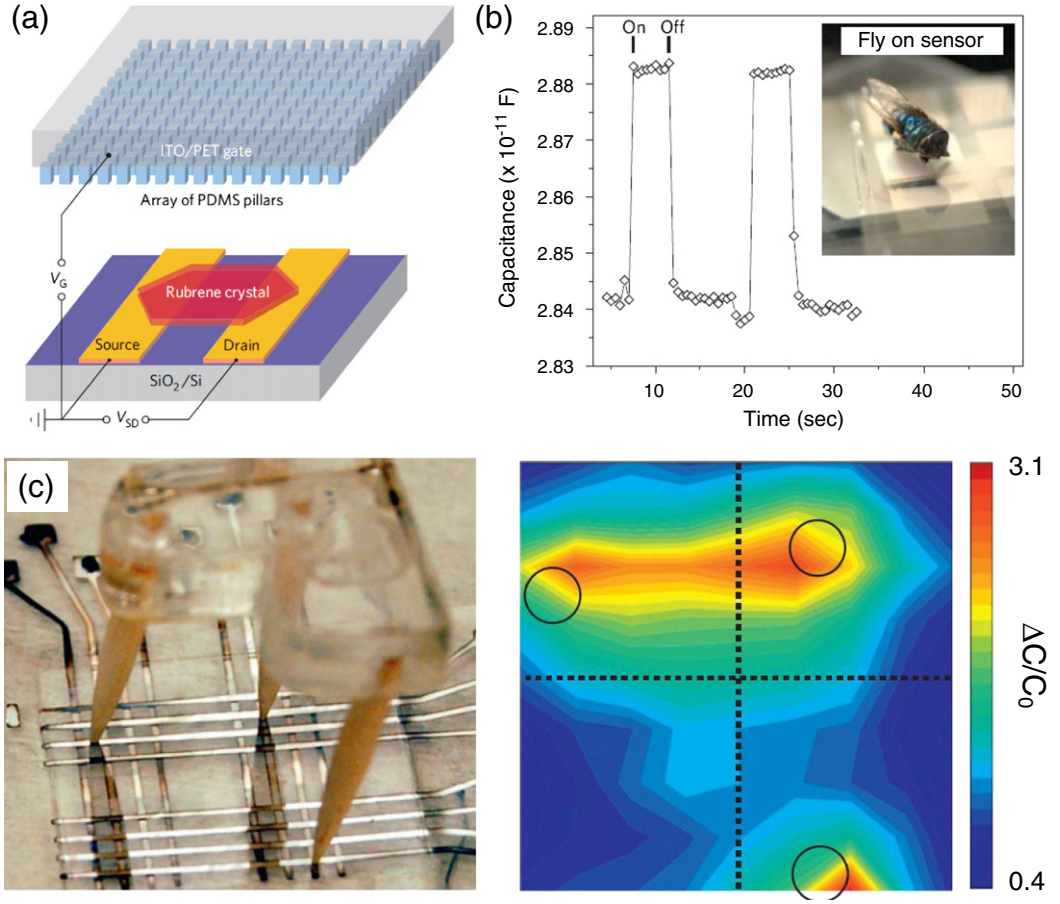

Fig. 8. (a) Schematic illustration of an OFET pressure sensor which consists of thin rubrene single crystals and microstructured PDMS dielectric films. (b) Capacitance change of the OFET pressure sensor when a bluebottle fly (~20 mg), corresponding to a pressure of 3 Pa, is placed and removed on a 64 mm^2 area. (c) "All-plastic" pixel-type pressure-sensor arrays (left) and their response to a tripod placed on top (right).

care and disease cure can be expected soon. Herein, we will introduce some of the latest achievements accomplished where nanomaterials on elastomeric substrates are used to explore new prospects in biological applications.

4.1. Visual prostheses

Blindness, whether congenital or stemming from age-related macular degeneration, is one of the most problematic issues that needs to be addressed, with approximately 30 million people suffering from blind-related diseases worldwide. However, and unfortunately, pharmaceutical treatments that can recover vision have not yet been developed, only some methods to delay the progression of age-related macular degeneration [139]. The retina is composed of multilayered tissues such as the inner limiting membrane, ganglion cells, photoreceptor cells, pigment epithelium, and choroid; during the course of defining the cause for blindness, it has been discovered that only the outer nuclear layers lose their function while the inner nuclear and retinal ganglion layers are partially preserved — up to approximately 80% of the neurons found in a normal eye remain active [140–142]. Hence, neural-prostheses that can electrically stimulate the surviving neurons may be viable as a vision-restoring methodology in retinal diseases [143,144] as illustrated in Fig. 11(a). A few initial reports have demonstrated that highly dense arrays of microelectrodes (MEAs) may serve as such a stimulus system [145–153], but there still exists too many barriers for these systems to have practical uses. The barriers include brain tissue injury, cerebrospinal fluid leakage, intracranial infection, and inability to replace a defective array.

For the realization of such visual prostheses, the most critical factors that must be addressed can be categorized as follows: a high density of MEAs and connecting wires that carry the stimulating signals to match with the numerous retinal cells, high flexibility to ensure conformal contact with an eyeball without damaging the tissues, and device biocompatibility. To increase the package integration density, the most widely adopted method is multilayer technology; however, this is not adequate for the fabrication of surgical implantation devices as multiple layers add to the thickness, thereby reducing the flexibility and increasing the probability of damaging the tissues during surgical implantation. Besides, it not only increases the overall fabrication cost, but also gives rise to reliability issues since multilayering reduces the thickness of the connecting wires.

Using a three-mask fabrication process, Chen et al. [154] proposed a new integrated connection method, in which the density of the connecting wires is significantly increased while maintaining the required flexibility. To ensure sustainable flexibility and biocompatibility at the same time, polyimide [155,156] was chosen as the substrate and insulation material of the exposed interconnect and electrodes, mainly composed of copper and gold. As can be seen in Fig. 11(b) and (c), a novel cross-shaped connecting design was implemented, which enabled increased connection density while maintaining flexibility and size. Through in vivo and in vitro experiments, they successfully revealed that the fabricated chips had no side-effects and are non-toxic to either direct cell contact or released soluble factors. This is shown through a survival rate test of the cultured cells with and without the chip using the Trypan blue exclusion method, along with the methyl blue tetrazolium enzyme reaction test to verify the

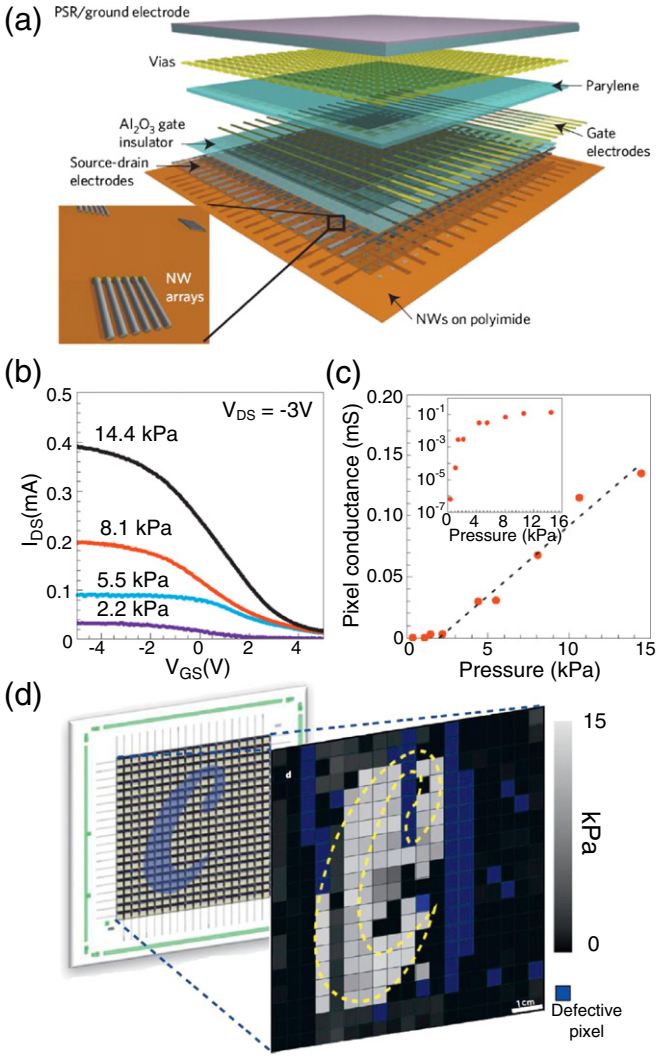

Fig. 9. (a) Layer-by-layer schematic illustration of a nanowire-based macroscale flexible pressure sensor. (b) Electrical characterization, showing I_{DS}–V_{GS} curves, of a NW-array sensor system. (c) Pressure dependence of the pixel output conductance as a function of strain. The inset is a log-scale plot. (d) Two-dimensional intensity profile, corresponding to the spot denoted by "C", showing that the applied pressure profile can be readily imaged.

cellular viability (Fig. 11(d)). Visual cortical cells cultured at 3, 7, 10, and 15 days with or without chips showed no significant difference in terms of both survival rates and cellular viabilities.

As previously mentioned, the concept of these visual prostheses is to stimulate an electrical signal from the MEAs to the remaining functional neuron cells. Here, an important consideration is the distal gap from a single microelectrode to the targeted retinal cells, which are located underneath a membrane layer to be stimulated. In specific, the ganglion cells are located under the inner limiting membrane and the photoreceptor cells are located under the choroid and pigment epithelium layer. Owing to the divergence of the electric field, the MEAs are expected to benefit more if the distal gap is small.

A novel 3D structure has been proposed by Koo et al. [157] that minimizes the distal gap between the MEAs and the retinal cells; they fabricated arrowhead-shaped microelectrodes that penetrate the membrane-structured tissue. Fig. 11(e) shows a schematic design of the visual prosthesis, which consists of the MEAs, a conductive line, and a connecting pad. Using the differential etching rate with respect to the crystal orientation of single-crystalline silicon in aqueous alkaline solutions, in combination with deep reactive ion etching, electroplating, and chemical mechanical polishing, the arrowhead-shaped MEAs were successfully fabricated on a flexible polyimide substrate. Uniformly-sized microelectrodes having sizes ranging from approximately 123.5 to 42 μm in height with post diameters of 130.5 to 16 μm were fabricated with high density (Fig. 11(f) left); Fig. 11(f) (right) shows a magnified image of the largest arrowhead-shaped microelectrode. The use of 3-D structured arrowhead-shaped MEAs not only led to a reduced distance from the MEAs to the target retinal cells, thereby lowering the threshold current, but also enabled a higher density array for higher resolution, larger surface area, and a longer device lifetime.

The issue of biocompatibility, which is important for preventing deterioration of both the electrode and neural tissues, was addressed by Bergonzo et al. [158]. Stimulation of the signals to the retinal neuron tissues requires injections of current from electronics to neural tissues, where the current must be transformed from electronic current into ionic current. During this process, which takes place at the electrode/tissue interface, oxidation/reduction of the electrode material occurs when negative/positive ions are translated from the tissue. The positive and negative currents introduced during a sequence of stimulations must be balanced in order not to degrade the electrode, and the amplitude of the stimulation current must be low enough to involve only reversible processes. If the electrode material impedes the injection of desired current, non-reversible reactions (e.g., hydrolysis of water contained in the tissue) occur which do harm to both the electrode and the neural tissue [146]. Furthermore, the material of choice for the metal electrodes has been passive metals such as iridium, platinum, and gold, which may be detrimental in that they do not provide an optimal contact to neurons; this might lead to the generation of reactive gliosis, producing an insulating surface between the implant and the neuron. As an alternative to those metal electrodes, nanocrystsalline diamond (NCD) was chosen as the electrode material in Bergonzo et al.'s work [159] owing to its extreme biocompatibility and stability in physiological media, and convenient processing methods using conventional CVD processes on large area substrates.

NCD microelectrode arrays having 3D geometries were readily fabricated using conventional silicon processing approaches, and then transferred onto polyimide substrates. Through evaluating the local variations of pH during symmetric current pulse injection tests, it has been shown that the NCD microelectrodes were capable of carrying higher charge injection fluxes of up to several hundred μC/cm^2, while the charge injection limit remained in the 10 to 100 μC/cm^2 range with Pt microelectrodes [160].

4.2. Controlled drug release and delivery

Controlled release of pharmaceutical drugs to desired positions at the correct time is considered to be one of the most effective methods to treat diseases requiring steady and accurate pharmaceutical treatments. Using nanoscience, the sustained release of medical molecules through a variety of drug-containing carriers is possible [161–164]. In a more complex manner, researchers sought a method to coordinate the input dosage and timing through external stimuli, including electric or magnetic fields [165–168], temperature [169,170], and changes in the surrounding pH value [171]. Although strain-driven stimulus is one of the most accommodating sources of input that can be easily triggered by a human body, little has been reported on the strained-controlled release of medical molecules owing to the lack of proper methodology to create a system in which such molecules would be safely encapsulated and react to a mechanical strain to be released. One possible solution would be to utilize patches that respond to body motions. In this respect, Hyun et al. [172] reported the fabrication of arrayed microcapsules, supported on an elastomeric PDMS substrate, which reply to mechanical strains to release the medical drugs encapsulated in the microcapsules.

The arrayed microcapsules were fabricated in the form of well-ordered buckled polymer thin films (polystyrene, PS) that provide

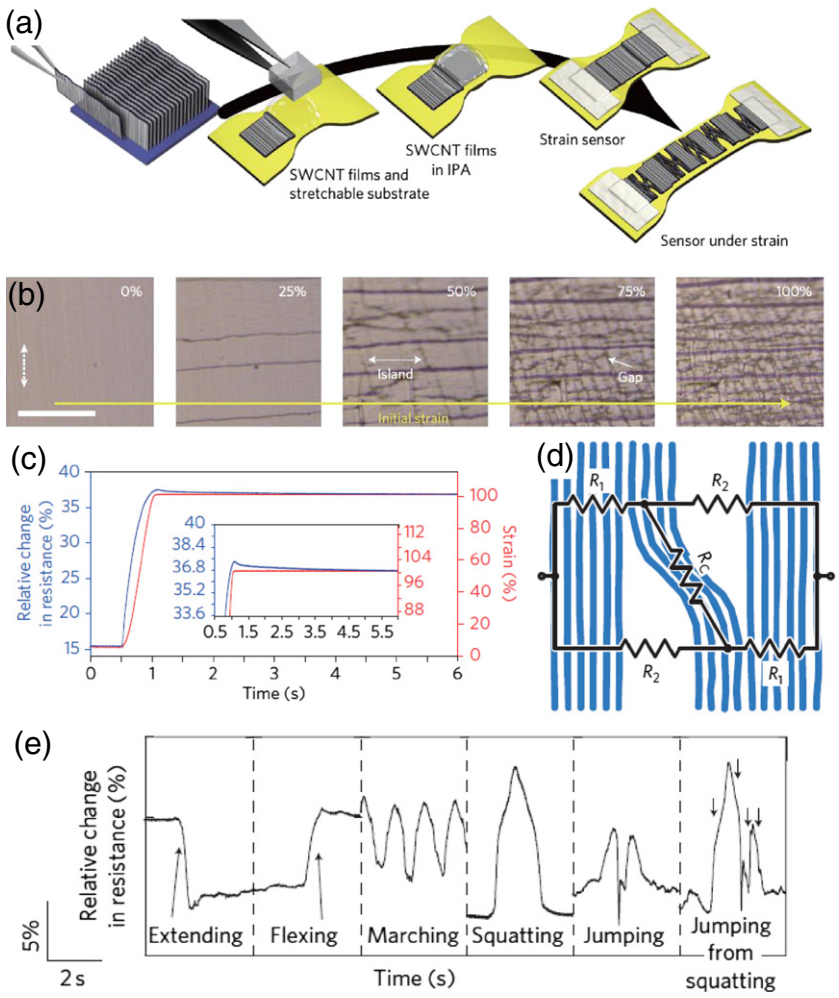

Fig. 10. (a) Fabrication process of a SWCNT strain sensor. (b) Optical images of the SWCNT film upon initial loading. The scar bar indicates 100 μm. (c) Relative change in resistance (blue) in response to a 5 to 100% step function increase in mechanical strain. Inset: close-up of the signal overshoot. (d) Model of the device circuit. (e) Relative changes in resistance versus time for human knee motions.

stretchability without defects. The arrays were spontaneously formed by depositing a PS layer on a thermally pre-strained elastomeric PDMS substrate as shown in Fig. 12(a). The target molecules were selectively loaded in the troughs of the buckled structure and they were tightly sealed once they were re-transferred to a new, softer elastomeric PDMS, leading to a form of encapsulation inside a microscale chamber structure. Hyun et al. [172] examined the amount of applicable strain that withstands the formation of cracks or peeling of the fabricated microcapsules upon repeated stretching and release; at a strain of 8.5% on the PDMS substrate, the microcapsule structures became completely flat. Strain levels higher than 8.5% led to the generation of cracks, while at a strain lower than 8.5%, the microcapsules returned to their original shape upon release of the strain. Fig. 12(b) shows atomic force microscopy (AFM) images of the microcapsules, depicting changes in dimensions as a result of mechanical stretching along the direction indicated by the white arrows.

The release behavior of the molecules from the microcapsules was also investigated; the dosage increased with the amount of strain induced on the microcapsules, while its amount was decreased during consecutive stretching and release events. Thus, the results indicate that the amount of released molecules can be controlled through adjusting the degree of strain. As a practical application, a strain-sensitive patch fabricated using hydrogel-patterned microcapsules was demonstrated (Fig. 12(c) and (d)) and attached to a human hand. By the motion of gripping and opening, the molecules were readily released from the patch.

While Hyun et al. [172] reported a possible means of utilizing mechanical strain as an input source to precisely control the release of target molecules, Tsioris et al. [173] investigated a rather more direct route of controlled-release drug delivery through transdermal administration using silk microneedles. In fact, microneedles have evolved as an efficient and pain-free mode for drug delivery, but have faced many limitations such as the inability to precisely control drug release kinetics, the possibility of local infection at the needle/skin interface, and lack of appropriate biomaterials. More importantly, the fabrication process of microneedle systems is often inadequate owing to elevated temperature and use of vacuum, which can be detrimental to temperature-sensitive drugs. In all, moving toward development of more sustainable microneedle systems requires the use of biocompatible, mechanically-robust materials that endure non-toxic products in vivo within a prescribed lifetime after application, better controllability of the drug-release behavior, and adoption of mild processing conditions to prevent damage to the incorporated vaccines while also supporting stabilization of the incorporated products to preserve efficacy during storage prior to use [174,175].

Tsioris et al. [173] used silk fibroin, an excellent biocompatible and biodegradable material [176,177] to create sustainable biopolymer microstructures having high aspect ratios that allow facile loading and controlled release of temperature-sensitive drugs. Fig. 13(a) illustrates the fabrication process of vaccine-loaded silk microneedles which can

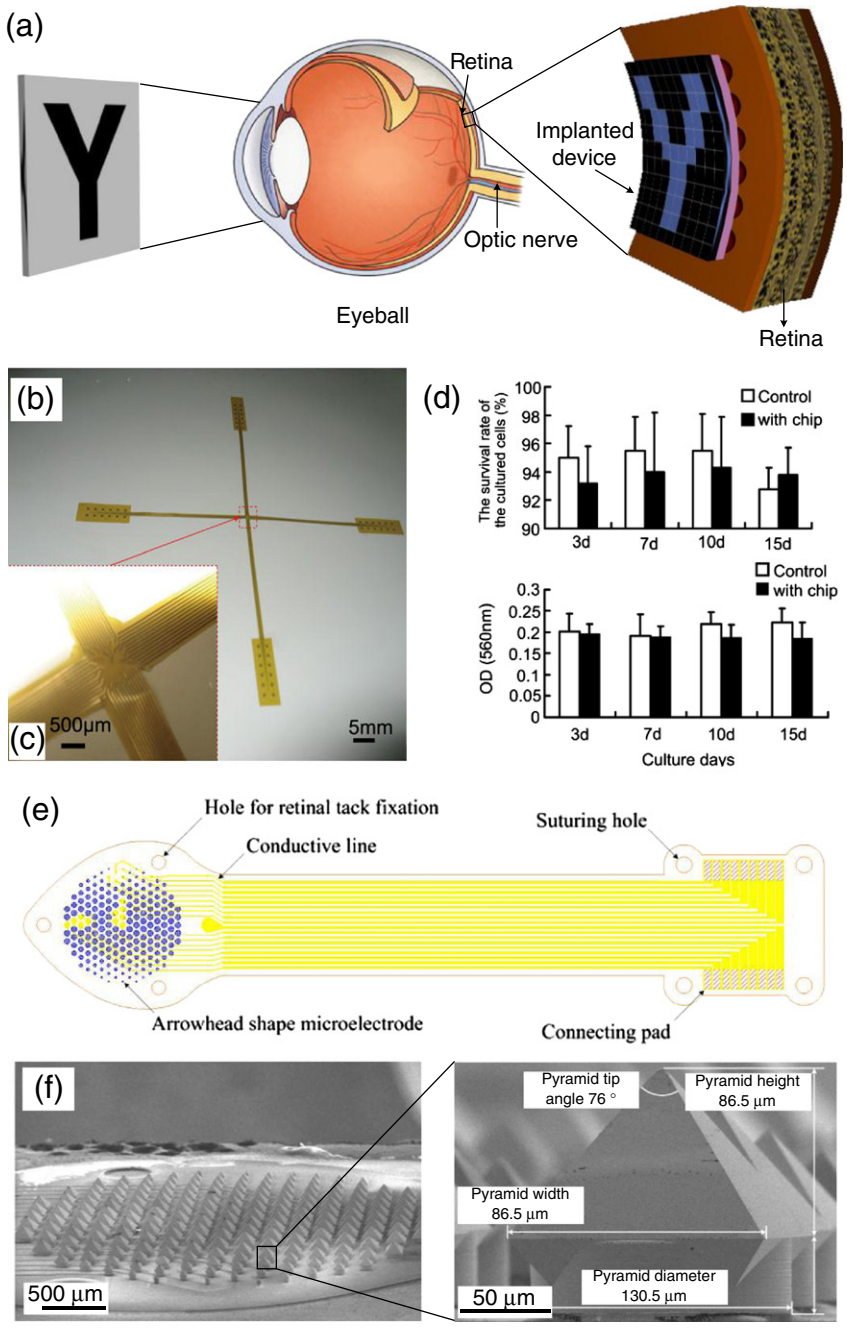

Fig. 11. (a) Schematic illustration conceptually showing how a visual prosthesis, implanted in the retina, functions. (b) An image of the stimulating electrode with four connector arms; (c) the inset shows a magnified image of the connection. (d) The survival rate and cellular viability of the cultured cells with and without the chip. (e) Design schematic of the visual prosthesis proposed by Koo et al. [157] consisting of MEAs, a conducting line, and a connecting pad. (f) SEM image of fabricated MEAs with a convex shape (left) and a magnified image of the largest arrowhead-shaped microelectrode (right).

be prepared at an ambient pressure and temperature. The negative PDMS mold derived from a micro-milled and chemically-etched aluminum microneedle was used to produce micron-scale silk needles loaded with pharmaceutical drugs. Fig. 13(b) shows the controlled enzymatic activities of the loaded drugs, horseradish peroxidase; a steady and sustained release of the loaded drugs is observed over a time interval of 2 h.

4.3. Bio-integrated circuits and electronic systems

Bio-integrated circuits can offer important opportunities for diagnosing and treating diseases, but a practical application that enables such functions is yet to be achieved. For example, cardiac arrhythmias can be properly treated if the irregular heart activities can be mapped in real-time by highly-distributed sensors over the surface of the heart. However, conventional tools use sparse arrays of rigid electrodes, usually arranged on a cylindrical catheter, manipulated from place to place to record from discrete sites on the heart; thus requiring iterative efforts with no capability of real-time monitoring [178,179]. As such, the major limitations in the integration of electronics to biological surfaces have been the hard, planar surfaces of semiconductors that are invasive in the soft, curvilinear surfaces of biological tissues, along with the instability of the electronic/biological interface that deteriorates both the device and the tissue health. High-performance electronics built on

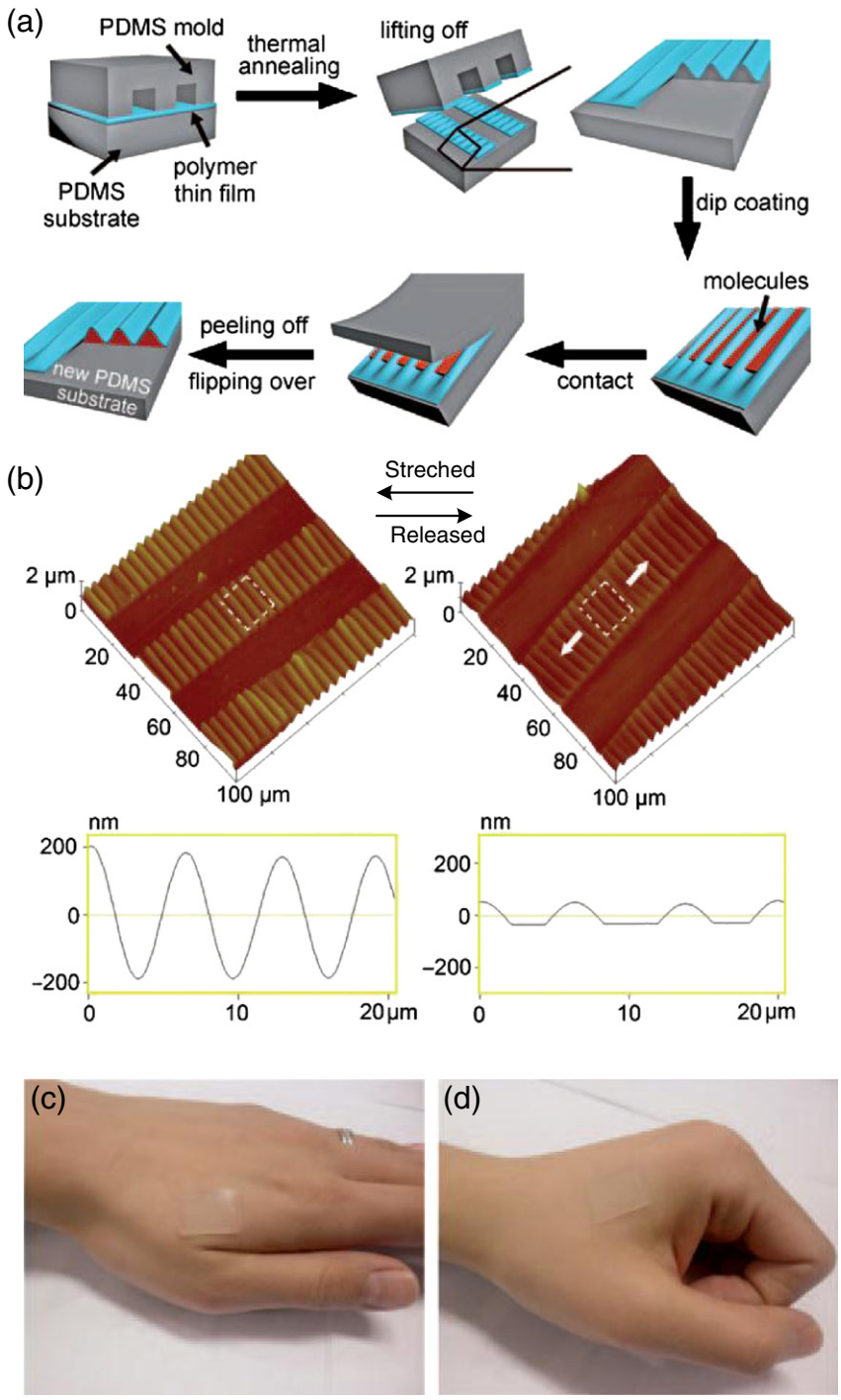

Fig. 12. (a) Process scheme for the preparation of arrayed microcapsules. (b) AFM images showing dimensions of the microcapsules with no strain applied (left) and with an applied strain of 6.5% (right). The bottom plots, (c) and (d), show hydrogel-patterned microcapsules with strain applied by opening and closing a human hand.

conventional semiconductor wafers are not suitable for intimate, non-invasive integration with the surfaces of biological tissues. In addition, they are vulnerable when in contact with saline solutions and biological fluids, leading to unwanted leakage currents that may damage the contacting tissues.

Recent work toward integrating electronics onto biological structures have thus focused on trying to improve the conformality of such electronic systems on the target tissues by means of reducing the thickness of the substrate or using stretchable, flexible substrates. Viventi et al. [180] demonstrated a working electronic device with high performance that is highly conformal to dynamic, living biological tissues, using ultrathin silicon nanoribbons on a bio-friendly flexible polyimide substrate. A total of 2016 n-type metal-oxide-semiconductor FETs were fabricated and divided into 288 unit cells, which comprise an amplifier, multiplexer, and electrode as shown in the circuit diagram of Fig. 14(a). The device is designed to detect and record electrical activity directly from the heart in vivo, where the 288 unit cells serve as the measurement points, spaced 800-μm apart and covering an area of 14.4 by 12.8 mm^2 (Fig. 14(b)). In their devices, the circuit was safely placed at the neutral mechanical plane in order to avoid damage from device

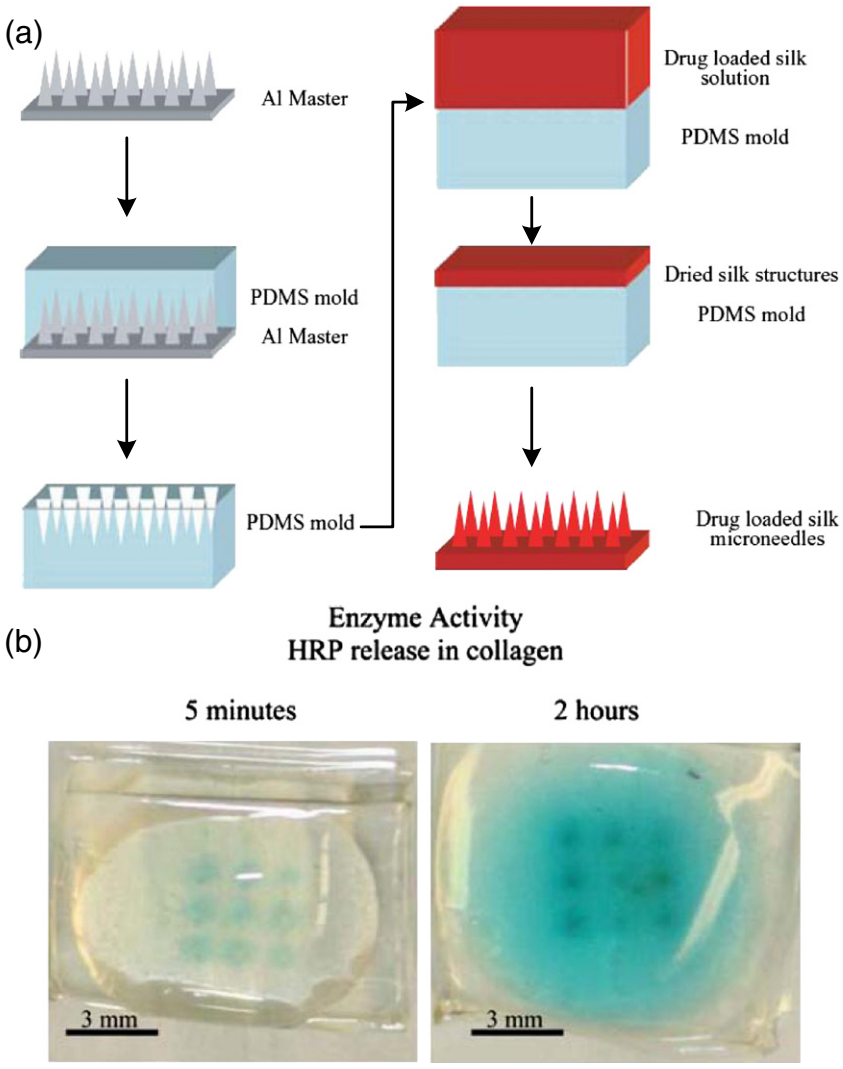

Fig. 13. (a) Process scheme for the fabrication of drug-loaded silk microneedles. (b) Images showing the enzymatic bioactivity, detected by a chromogenic substrate, of the loaded drugs 5 min and 2 h following release.

distortion and from intrusion of biofluids. In vivo experiments performed in the hearts of Yorkshire pigs confirmed that the device naturally adhered to the curved cardiac tissue with excellent conformality, even during rapid cardiac pacing. The blue lines in Fig. 14(c) depict dynamic variations in the surface shape associated with maintaining conformal contact. Reliable data could be retrieved over the course of some ten thousand bending cycles from all 288 electrodes. Based on the recorded unipolar voltage data, a color image was plotted that represents wavefront propagation showing cardiac activation moving from the left side of the array to the right side (Fig. 14(d)). This conformal, bio-interfaced active electronic system on a flexible plastic substrate provides a basis for practical implantable devices that surmount the difficulties associated with integration of electronic devices on the curvilinear, complex environment of living human tissues.

Oftentimes, the use of a flexible substrate fails to provide ultrahigh conformality between the interface of an electronic system and a living tissue, as the surfaces of a living tissue can be quite convoluted and rugged, such as that of a brain. It is thus required to reduce the thickness of the substrate to a few μm, which can greatly decrease the bending rigidity and improve conformal contact. However, ultrathin geometries under 10 μm are impractical in conventional designs because the films cannot be handled effectively during fabrication or implantation due to insufficient self-supporting properties.

Kim et al. [181] overcame the difficulties of fabricating an ultrathin electronic device by using a silk supporting substrate, which can be dissolved after its integration onto a biological tissue (in their report, a feline brain) using saline solution, and showed that the device forms an excellent conformal contact with the brain. Fig. 15(a) schematically illustrates the integration process of electrode arrays designed for passive neural recording on a feline brain. Briefly, ultrathin films of polyimide are spin-cast onto silicon wafers coated with sacrificial layers of PMMA as a support membrane for neural recording electrode arrays; they were then transfer-printed onto a silk substrate, and an anisotropic conductive film (ACF) was bonded to one end of the electrode pads to provide an electrical connection to external data acquisition systems. Finally, the device was brought into contact with the brain, and the silk support dissolved by saline solution, leading to the full integration of the ultrathin device on the brain.

The degree of conformality was tested using varying thicknesses of the polyimide membrane; three different samples were prepared using 76- and 2.5-μm-thick polyimide films, and a mesh-structured 2.5-μm-thick polyimide film. The photographs in Fig. 15(b) to (d) clearly show that excellent conformality can be achieved when the polyimide support has a 2.5-μm-thick mesh structure. This is also in good accordance with the corresponding average evoked electrode response measurements located below the photographs. The colors show the ratio of the rms amplitude

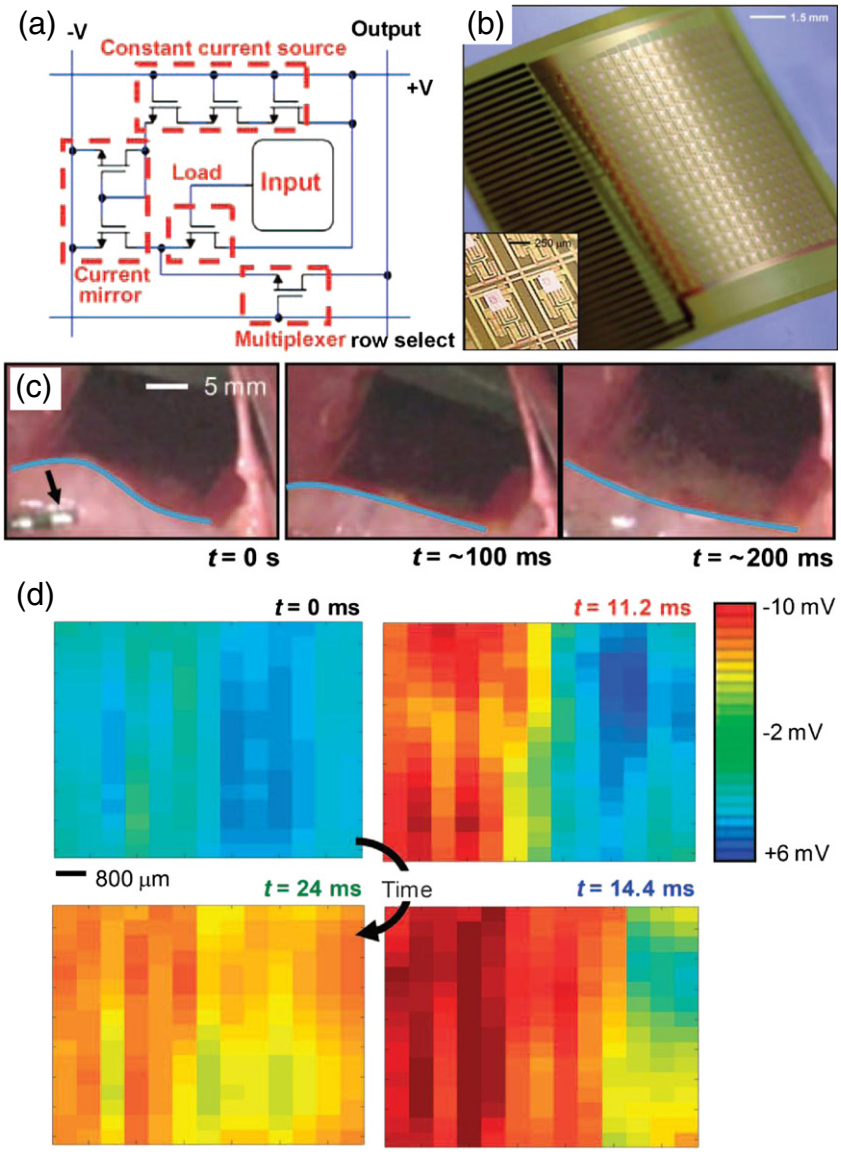

Fig. 14. (a) Circuit design of an active, flexible device for cardiac electrophysiological mapping. (b) Photographic image of the fabricated device in a slightly bent state; the inset shows a magnified view of a pair of unit cells. (c) Sequential images during the contraction cycle of the heart. Blue lines emphasize the degree of bending along the device. The black arrow in the left-most image indicates a conventional pacing electrode. (d) Representative voltage data, recorded from four points using a flexible electrophysiology mapping device, showing normal cardiac wavefront propagation. The color scale in the upper right corresponds to the voltages retrieved.

of each average electrode response in the 200 ms window, with the scale of the rms amplitude at the bottom of Fig. 15(d). Whereas weak signals with low outputs could be retrieved from the electrodes fabricated on 76- and 2.5-μm-thick polyimide films, indicated by the yellowish to orange colors, reliable data was obtained using the ultrahigh conformal electrodes fabricated on mesh-structured 2.5-μm-thick polyimide film, represented by green in the color map. Although only passive electrode systems were demonstrated, this technology provides a novel route toward intimate electronic integration in which a reliable biotic/abiotic interface is achieved on living, moving biological structures. This is essential for implanted, high-resolution medical devices.

In the following year, Kim et al. [182] demonstrated a new type of electronics that conformally laminates onto the surface of the skin. Distinctively, an entire system of electrodes, sensors, power supply, and communication components was integrated. Fig. 16(a) is a representative image of a platform for multifunctional electronics having physical properties matched to the epidermis. The concept used in this work was similar to their previous work [174] in that the multifunctional electronic system was conformally laminated onto the skin by dissolving the support. The difference is in the materials used for the support and the membrane upon which the actual components were fabricated. Here, the multifunctional sensors, light-emitting diodes, active/passive circuit elements, wireless power coils, and devices for radio frequency communications were all built on the surface of a gas-permeable elastomeric sheet of modified silicone, with a low Young's modulus of ~60 kPa and thickness of ~30 μm. For the temporary support to mount these systems on the skin, a water-soluble polyvinyl alcohol sheet with thickness of ~50 μm is used.

Fig. 16(b) illustrates the multifunctional epidermal electronic system on skin, showing its undeformed, compressed, and stretched state. It can be seen that the overall construct resembles that of a temporary transfer tattoo, where the robust adhesion to the skin was accomplished via van der Waals forces alone, without the aid of a separate adhesive layer. In all, the multifunctional electronic systems were used to successfully

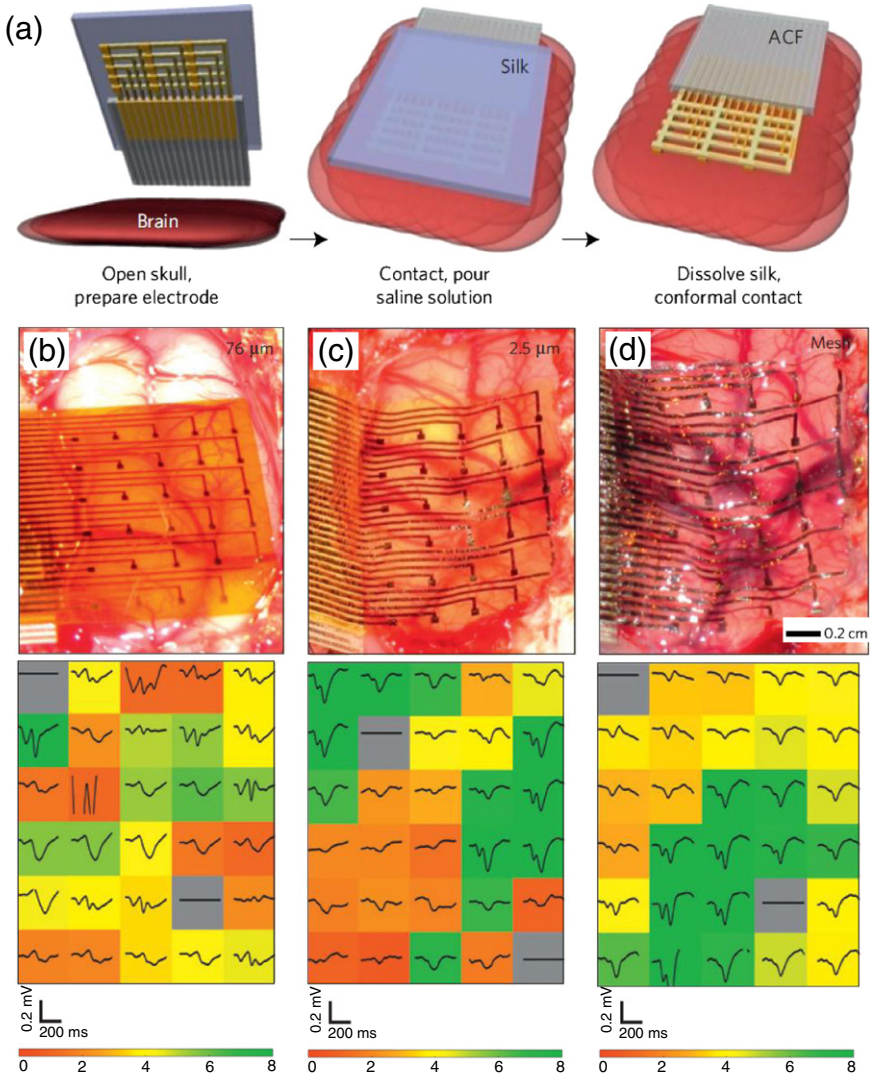

Fig. 15. (a) Schematic illustration of the steps for implanting PI electrode arrays with a dissolvable silk support. (b)–(d) Photographic images and the corresponding average evoked response from each electrode implanted on a feline brain with (b) 76-μm, (c) 2.5-μm, (d) and 2.5-μm-mesh electrode arrays.

measure the electrical activity produced by the heart, brain, and skeletal muscles. The details are not covered in this section, but the materials and mechanics demonstrated in Kim et al.'s work can definitely lead to a new route for integration of perfectly conformal, intimate and reliably attached high-performance electronic systems on the surfaces of living biological tissues with much less potential harm than previously reported methods.

5. Conclusion

Whereas the major research on flexible electronics for the past few decades has been focused on the discovery and development of new materials, fabrication techniques, and investigation of the properties of these materials in correlation with compliant substrates, most recent research focuses on methods to deliver novel functions. This article reviews recent efforts and advancements that successfully overcome or circumvent the constraints of conventional flat technology, covering the materials used, device design, implementation methods, working principles, and performance metrics.

Although much is understood concerning the underlying mechanisms and capabilities of stretchable and flexible devices through comprehensive experimental and theoretical studies, the following issues must be addressed before the commercialization of fully integrated flexible systems is sustainable. First is the development of a new support or substrate that can endure high levels of strain; considering that the size of the active elements on such substrates are in the range of nanometers, even a micro-crack would severely affect device performance. Secondly, a method to overcome changes in the materials and electronic properties in the deformed state is required; the performance level must be maintained under bent or curved states, and a steady output should be achieved with minimal variation. A significant amount of deviation in the device performance means that it is vulnerable to stress, and repeated exertion of stress can lead to device breakdown. The third issue is associated with the fabrication of identical devices over large areas; as a flexible device can often be fabricated through a bottom-up approach, the alignment of the nanomaterials must be handled well as mentioned in Section 3. This is extremely difficult, considering that the nanomaterials synthesized using the same experimental conditions may exhibit dissimilar properties. Lastly, the problem of residual stress needs to be addressed; even the most robust materials are subject to abrasion after thousands of bending and folding events due to the accumulated external/internal stresses and the residual stress can affect the device performance, giving rise to reliability issues. Nonetheless, the seemingly limitless potentials of flexible

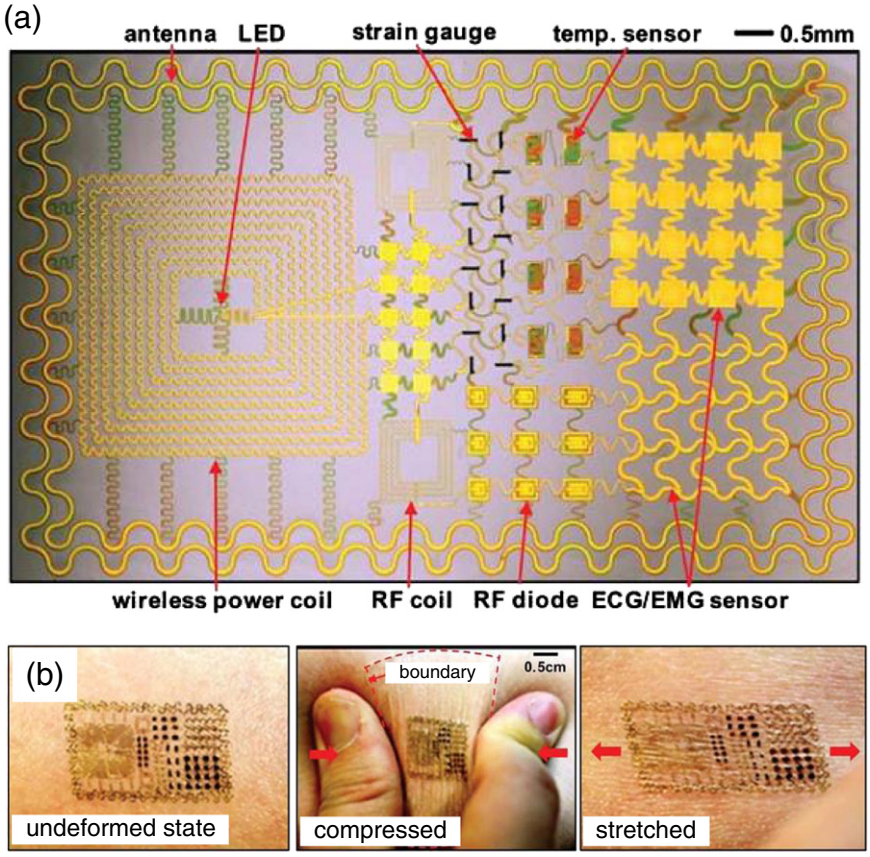

Fig. 16. (a) Image of a multifunctional electronic system with physical properties matched to the human skin. (b) Undeformed (left), compressed (middle), and stretched (right) states of a fabricated device conformally attached to the skin through van der Waals forces.

electronics have drawn global interest, and with the ongoing increase in the demand for more convenient, smarter applications, opportunities in the area of flexible electronics using nanomaterials appear almost inexhaustible.

Acknowledgement

This study was supported in part by the Priority Research Centers Program through the National Research Foundation of Korea (NRF) funded by the Ministry of Education, Science and Technology (MEST) (2012-0006689) and the Converging Research Center Program through the Ministry of Education, Science and Technology (2012K001321). This work was also supported by the National Research Foundation of Korea(NRF) grant funded by the Korea government (MEST) (No. 2011-0028594).

References

[1] J.A. Rogers, Z. Bao, K. Baldwin, A. Dodabalapur, B. Crone, V.R. Raju, V. Kuck, H. Katz, K. Amundson, J. Ewing, P. Drzaic, Proc. Natl. Acad. Sci. 98 (2001) 4835.
[2] G.H. Gelinck, H.E.A. Huitema, E.V. Veenendaal, E. Cantatore, L. Schrijnemakers, J.B.P.H. Van Der Putten, T.C.T. Geuns, M. Beenhakkers, J.B. Giesbers, B.-H. Huisman, E.J. Meijer, E.M. Benito, F.J. Touwslager, A.W. Marsman, B.J.E. Van Rens, D.M. De Leeuw, Nat. Mater. 3 (106) (2004).
[3] P. Avouris, Z. Chen, V. Perebeinos, Nat. Nanotechnol. 2 (2007) 605.
[4] A.G. MacDiarmid, Angew. Chem. Int. Ed. 40 (2001) 2581.
[5] A.J. Heeger, Angew. Chem. Int. Ed. 40 (2001) 2591.
[6] F. Hussain, M. Hojjati, M. Okamoto, R.E. Gorga, J. Compos. Mater. 40 (2006) 1511.
[7] J. Cho, A.R. Boccaccini, M.S.P. Shaffer, J. Mater. Sci. 44 (2009) 1934.
[8] D.R. Paul, L.M. Robeson, Polymer 49 (2008) 3187.
[9] Z. Fan, J.C. Ho, T. Takahashi, R. Yerushalmi, K. Takei, A.C. Ford, Y.-L. Chueh, A. Javey, Adv. Mater. 21 (2009) 3730.
[10] Q. Cao, J.A. Rogers, Adv. Mater. 21 (2009) 29.
[11] Z. Bao, Adv. Mater. 12 (3) (2000) 227.
[12] A.P. Quist, E. Pavlovic, S. Oscarsson, Anal. Bioanal. Chem. 381 (2005) 591.
[13] J.A. Rogers, R.G. Nuzzo, Mater. Today 9 (2006) 32.
[14] G. Eda, G. Fanchini, M. Chhowalla, Nat. Nanotechnol. 3 (2008) 270.
[15] S.H. Ko, H. Pan, C.P. Grigoropoulos, C.K. Luscombe, J.M. Frechet, D. Poulikakos, Nanotechnology 18 (2007) 345202.
[16] E. Menard, K.J. Lee, D.-Y. Khang, R.G. Nuzzo, J.A. Rogers, Appl. Phys. Lett. 84 (2004) 5398.
[17] R.A. Street, W.S. Wong, S.E. Ready, M.L. Chabinyc, A.C. Arias, S. Limb, A. Salleo, R. Lujan, Mater. Today 9 (2006) 32.
[18] D.-H. Kim, J.A. Rogers, Adv. Mater. 20 (2008) 4887.
[19] J.A. Rogers, Y. Huang, Proc. Natl. Acad. Sci. 106 (2009) 10875.
[20] M.J. Cordill, J. Miner. Met. Mater. Soc. 62 (9) (2010).
[21] S. Logothetidis, Mater. Sci. Eng. B 152 (2008) 96.
[22] Y. Sun, J.A. Rogers, Adv. Mater. 19 (2007) 1897.
[23] J.A. Rogers, T. Someya, Y. Huang, Science 327 (2010) 1603.
[24] M.-C. Choi, Y. Kim, C.-S. Ha, Prog. Polym. Sci. 33 (2008) 581.
[25] A. Nathan, B.R. Chalamala, Proc. IEEE 93 (2005) 1235.
[26] A. Nathan, B.R. Chalamala, Proc. IEEE 93 (2005) 1391.
[27] J.A. Paradiso, T. Starner, IEEE Pervasive Comput. 4 (2005) 18.
[28] J.-M. Tarascon, M. Armand, Nature 414 (2001) 359.
[29] A.S. Aricó, P. Bruce, B. Scrosati, J.-M. Tarascon, W. van Schalkwijk, Nat. Mater. 4 (2005) 366.
[30] J. Kymissis, C. Kendall, J. Paradiso, N. Gershenfeld, in: Proc. 2nd IEEE Int. Symp. Wearable Computers, Pitsburgh, 1998, p. 132.
[31] N.S. Shenck, J.A. Paradiso, IEEE Micro 21 (2001) 30.
[32] L.C. Rome, L. Flynn, E.M. Goldman, T.D. Yoo, Science 309 (2005) 1725.
[33] S.R. Platt, S. Farritor, K. Garvin, H. Haider, IEEE/ASME Trans. Mechatron. 10 (2005) 240.
[34] K.A. Cook-Chennault, N. Thambi, M.A. Bitetto, E.B. Hameyie, Bull. Sci. Technol. Soc. 28 (2008) 496.
[35] D.A. Scrymgeour, J.W.P. Hsu, Nano Lett. 8 (2008) 2204.
[36] S. Priya, D.J. Inman, Energy Harvesting Technologies, Springer, 2009.
[37] L.M. Swallow, J.K. Luo, E. Siores, I. Patel, D. Dodds, Smart Mater. Struct. 17 (2008) 025017.
[38] X. Chen, J. Li, G. Zhang, Y. Shi, Adv. Mater. 23 (2011) 3965.
[39] E. Venkatragavaraj, B. Satish, P.R. Vinod, M.S. Vijaya, et al., J. Phys. D: Appl. Phys. 34 (2001) 487.
[40] G. Rujijanagul, S. Boonyakul, T. Tunkasiri, J. Mater. Sci. Lett. 20 (2001) 1943.
[41] M.-H. Zhao, Z.-L. Wang, S.X. Mao, Nano Lett. 4 (2004) 587.
[42] Y. Yang, W. Guo, X. Wang, Z. Wang, J. Qi, Y. Zhang, Nano Lett. 12 (2012) 1919.

[43] S.R. Anton, H.A. Sodano, Smart Mater. Struct. 16 (2007).
[44] T. Rödig, A. Schönecker, J. Am. Ceram. Soc. 93 (2010) 901.
[45] Y. Qi, M.C. McAlpine, Energy Environ. Sci. 3 (2010) 1275.
[46] J.M. Kim, ECS Trans. 35 (2011) 5.
[47] A.A. Barlian, W.-T. Park, J.R. Mallon Jr., A.J. Rastegar, B.L. Pruitt, Proc. IEEE 97 (2009) 514.
[48] H.A. Sodano, D.J. Inman, G. Park, Shock Vib. Dig. 36 (2004) 197.
[49] A. Preumont, Mechatronics: Dynamics of Electromechanical and Piezoelectric Systems, Springer, 2006.
[50] J. van Randeraat, R.E. Setterington, Piezoelectric Ceramics, Mullard, 1974.
[51] S. Xu, Y. Qin, C. Xu, Y. Wei, R. Yang, Z.L. Wang, Nat. Nanotechnol. 5 (2010) 366.
[52] R. Yang, Y. Qin, L. Dai, Z.L. Wang, Nat. Nanotechnol. 4 (2009) 34.
[53] Y. Qi, N.T. Jafferis, K. Lyons Jr., C.M. Lee, H. Ahmad, M.C. McAlpine, Nano Lett. 10 (2010) 524.
[54] S. Xu, B.J. Hansen, Z.L. Wang, Nat. Commun. 1 (2010) 93.
[55] C. Chang, V.H. Tran, J. Wang, Y.-K. Fuh, L. Lin, Nano Lett. 10 (2010) 726.
[56] O. Guillon, F. Thiebaud, D. Perreux, Int. J. Fract. 117 (2002) 235.
[57] T.D. Nguyen, J.M. Nagarah, Y. Qi, S.S. Nonnenmann, A.V. Morozov, S. Li, C.B. Arnold, M.C. McAlpine, Nano Lett. 10 (2010) 4595.
[58] C.R. Martin, I.A. Aksay, J. Phys. Chem. B 107 (2003) 4261.
[59] K.-I. Park, S. Xu, Y. Liu, G.-T. Hwang, S.-J.L. Kang, Z.L. Wang, K.J. Lee, Nano Lett. 10 (2010) 4939.
[60] J.E. Spanier, A.M. Kolpak, J.J. Urban, I. Grinberg, L. Ouyang, W.S. Yun, A.M. Rappe, H. Park, Nano Lett. 6 (2006) 735.
[61] Y. Qi, J. Kim, T.D. Nguyen, B. Lisko, P.K. Purohit, M.C. McAlpine, Nano Lett. 11 (2011) 1331.
[62] X. Chen, S. Xu, N. Yao, Y. Shi, Nano Lett. 10 (2010) 2133.
[63] M. Lee, C.-Y. Chen, S. Wang, S.N. Cha, Y.J. Park, J.M. Kim, L.-J. Chou, Z.L. Wang, Adv. Mater. 24 (2012) 1759.
[64] L. Vayssieres, Adv. Mater. 15 (2003) 464.
[65] Z.W. Pan, Z.R. Dai, Z.L. Wang, Science 291 (2001) 1947.
[66] S. Xu, Z.L. Wang, Nano Res. 4 (2011) 1013.
[67] P. Du, G. O'Grady, J.U. Egbuji, W.J. Lammers, D. Budgett, P. Nielsen, J.A. Windsor, A.J. Pullan, L.K. Cheng, Ann. Biomed. Eng. 37 (2009) 839.
[68] A.M. Morales, C.M. Lieber, Science 279 (1998) 208.
[69] H. Kind, H. Yan, B. Messer, M. Law, P. Yang, Adv. Mater. 14 (2002) 158.
[70] Y. Xia, P. Yang, Y. Sun, Y. Wu, B. Mayers, B. Gates, Y. Yin, F. Kim, H. Yan, Adv. Mater. 15 (5) (2003) 354.
[71] K.H. An, S.Y. Jeong, H.R. Hwang, Y.H. Lee, Adv. Mater. 16 (2004) 1005.
[72] Y. Im, C. Lee, R.P. Vasquez, M.A. Bangar, N.V. Myung, E.J. Menke, R.M. Penner, M. Yun, Small 2 (3) (2006) 356.
[73] H.-W. Ra, K.-S. Choi, J.-H. Kim, Y.-B. Hahn, Y.-H. Im, Small 4 (8) (2008) 1105.
[74] J. Kong, N.R. Franklin, C. Zhou, M.G. Chapline, S. Peng, K. Cho, H. Dai, Science 287 (2000) 622.
[75] Y. Cui, C.M. Lieber, Science 291 (2001) 851.
[76] M.C. McAlpine, H. Ahmad, D. Wang, J.R. Heath, Nat. Mater. 6 (2007) 379.
[77] J. Zhou, Y. Gu, P. Fei, W. Mai, Y. Gao, R. Yang, G. Bao, Z.L. Wang, Nano Lett. 8 (2008) 3035.
[78] C.-S. Woo, C.-H. Lim, C.-W. Cho, B. Park, H. Ju, D.-H. Min, C.-J. Lee, S.-B. Lee, Microelectron. Eng. 84 (2007) 1610.
[79] M.T. Kelly, J.K.M. Chun, A.B. Bocarsly, Nature 382 (1996) 214.
[80] H.J. In, C.R. Field, P.E. Pehrsson, Nanotechnology 22 (2011) 355501.
[81] R.B. Sadeghian, M.S. Islam, Nat. Mater. 10 (2011) 135.
[82] D.N. Ventura, S. Li, C.A. Baker, C.J. Breshike, A.L. Spann, G.F. Strouse, H.W. Kroto, S.F.A. Acquah, Carbon 50 (2012) 2666.
[83] D.R. Kauffman, A. Star, Angew. Chem. Int. Ed. 47 (2008) 6550.
[84] H.Y. Jeong, D.-S. Lee, H.K. Choi, D.H. Lee, J.-E. Kim, J.Y. Lee, W.J. Lee, S.O. Kim, S.-Y. Choi, Appl. Phys. Lett. 96 (2010) 213105.
[85] C.E. Cava, R.V. Salvatierra, D.C.B. Alves, A.S. Ferlauto, A.J.G. Zarbin, L.S. Roman, Carbon 50 (2012) 1953.
[86] Y. Liu, X. Dong, P. Chen, Chem. Soc. Rev. 41 (2012) 2283.
[87] K.R. Ratinac, W. Yang, S.P. Ringer, F. Braet, Environ. Sci. Technol. 44 (2010) 1167.
[88] L. Guo, H.-B. Jiang, R.-Q. Shao, Y.-L. Zhang, S.-Y. Xie, J.-N. Wang, X.-B. Li, F. Jiang, Q.-D. Chen, T. Zhang, H.-B. Sun, Carbon 50 (2012) 1667.
[89] Y. Yao, X. Chen, H. Guo, Z. Wu, X. Li, Sens. Actuators B 161 (2012) 1053.
[90] H. Ahn, H.C. Wikle III, S.-B. Kim, D. Liu, S. Lee, M. Park, D.-J. Kim, J. Electrochem. Soc. 159 (2012) E23.
[91] M.A. Lim, D.H. Kim, C.-O. Park, Y.W. Lee, S.W. Han, Z. Li, R.S. Williams, I. Park, ACS Nano 6 (2012) 598.
[92] C.-Y. Lee, C.-C. Chang, Y.-M. Lo, Sensors 10 (2010) 10701.
[93] K.J. Choi, H.W. Jang, Sensors 10 (2010) 4083.
[94] G. Korotcenkov, B.K. Cho, Sens. Actuators B 161 (2012) 28.
[95] P. Hidalgo, R.H.R. Castro, A.C.V. Coelho, D. Gouvêa, Chem. Mater. 17 (2005) 4149.
[96] M. Seetha, P. Meena, D. Mangalaraj, Y. Masuda, K. Senthil, Mater. Chem. Phys. 133 (2012) 47.
[97] G. Kiriakidis, K. Moschovis, I. Kortidis, R. Skarvelakis, J. Sens. 2009 (2009) 727893.
[98] M.-T. Ke, M.-T. Lee, C.-Y. Lee, L.-M. Fu, Sensors 9 (2009) 2895.
[99] S.R. Aliwell, J.F. Halsall, K.F.E. Pratt, J. O'Sullivan, R.L. Jones, R.A. Cox, S.R. Utembe, G.M. Hansford, D.E. Williams, Meas. Sci. Technol. 12 (2001) 684.
[100] T. Samerjai, N. Tamaekong, C. Liewhiran, A. Wisitsoraat, A. Tuantranont, S. Phanichphant, Sens. Actuators B 157 (2011) 290.
[101] L. Wang, J. Pfeifer, C. Balázsi, P.I. Gouma, Mater. Manuf. Processes 22 (2007) 773.
[102] M. Righettoni, A. Tricoli, S.E. Pratsinis, Anal. Chem. 82 (2010) 3581.
[103] S.L. Bai, R.X. Luo, B.J. Shi, Z.Y. Liu, D.Q. Li, A.F. Chen, IEEE Sens. J. 10 (2010) 1633.
[104] Y.J. Choi, Z. Seeley, A. Bandyopadhyay, S. Bose, S.A. Akbar, Sens. Actuators B 124 (2007) 111.
[105] D. Morris, R.G. Egdell, J. Mater. Chem. 11 (2001) 3207.
[106] M. Ferroni, V. Guidi, G. Martinelli, G. Faglia, P. Nelli, G. Sberveglieri, NanoStruct. Mater. 7 (1996) 709.
[107] H.-M. Lin, T.-Y. Hsu, C.-Y. Tung, C.-M. Hsu, NanoStruct. Mater. 6 (1995) 1001.
[108] I.-D. Kim, A. Rothschild, D.-J. Yang, H.L. Tuller, Sens. Actuators B 130 (2008) 9.
[109] M.C. Carotta, M. Ferroni, D. Gnani, V. Guidi, M. Merli, G. Martinelli, M.C. Casale, M. Notaro, Sens. Actuators B 58 (1999) 310.
[110] M.R. Mohammadi, D.J. Fray, M.C. Cordero-Cabrera, Sens. Actuators B 124 (2007) 74.
[111] H. Tang, K. Prasad, R. sanjinés, F. Lévy, Sens. Actuators B 26 (1995) 71.
[112] B. Karunagaran, P. Uthirakumar, S.J. Chung, S. Velumani, E.-K. Suh, Mater. Charact. 58 (2007) 680.
[113] C. Garzella, E. Comini, E. Tempesti, C. Frigeri, G. Sberveglieri, Sens. Actuators B 68 (2000) 189.
[114] G.-L. Tan, X.-J. Wu, Thin Solid Films 330 (1998) 59.
[115] K.-I. Shimizu, K. Kashiwagi, H. Nishiyama, S. Kakimoto, S. Sugaya, H. Yokoi, A. Satsuma, Sens. Actuators B 130 (2008) 707.
[116] Z. Zhang, C. Zhang, X. Zhang, Analyst 127 (2002) 792.
[117] A.M. Azad, S.G. Mhaisalkar, L.D. Birkefeld, S.A. Akbar, K.S. Goto, J. Electrochem. Soc. 139 (1992) 2913.
[118] W. Xiong, G.M. Kale, ECS Trans. 1 (2006) 151.
[119] H.-I. Chen, Y.-I. Chou, C.-Y. Chu, Sens. Actuators B 85 (2002) 10.
[120] K. Luongo, A. Sine, S. Bhansali, Sens. Actuators B 111 (2005) 125.
[121] B. Sutapun, M. Tabib-Azar, A. Kazemi, Sens. Actuators B 60 (1999) 27.
[122] E. Lee, J.M. Lee, J.H. Koo, W. Lee, T. Lee, Int. J. Hydrogen Energy 35 (2010) 6984.
[123] S. Lee, J. Hong, J.H. Koo, S. Lee, K. Lee, S. Im, T. Lee, IEEE Trans. Electron Devices 58 (2011) 3329.
[124] J.-H. Ahn, H.-S. Kim, K.J. Lee, S. Jeon, S.J. Kang, Y. Sun, R.G. Nuzzo, J.A. Rogers, Science 314 (2006) 1754.
[125] T. Shimoda, S. Inoue, S. Utsunomiya, Proc. SPIE 4295 (2001) 52.
[126] M.C. McAlpine, H. Ahmad, D. Wang, J.R. Heath, Nat. Mater. 6 (2007) 379.
[127] H.Y. Jeong, D.-S. Lee, H.K. Choi, D.H. Lee, J.-E. Kim, J.Y. Lee, W.J. Lee, S.O. Kim, S.-Y. Choi, Appl. Phys. Lett. 96 (2010) 213105.
[128] J. Yi, J.M. Lee, W.I. Park, Sens. Actuators B 155 (2011) 264.
[129] J. Lee, W. Shim, E. Lee, J.S. Noh, W. Lee, Angew. Chem. 123 (2011) 5413.
[130] H.R. Nicholls, M.H. Lee, Int. J. Rob. Res. 8 (1989) 3.
[131] M.H. Lee, H.R. Nicholls, Mechatronics 9 (1999) 1.
[132] S.C.B. Mannsfeld, B.C.-K. Tee, R.M. Stoltenberg, C.V.H.-H. Chen, S. Barman, B.V.O. Muir, A.N. Sokolov, C. Reese, Z. Bao, Nat. Mater. 9 (2010) 859.
[133] C. Metzger, Appl. Phys. Lett. 92 (2008) 013506.
[134] I. Manunza, A. Sulis, A. Bonfiglio, Appl. Phys. Lett. 89 (2006) 143502.
[135] K. Takei, T. Takahashi, J.C. Ho, H. Ko, A.G. Gillies, P.W. Leu, R.S. Fearing, A. Javey, Nat. Mater. 9 (2010) 821.
[136] T. Someya, T. Sekitani, S. Iba, Y. Kato, H. Kawaguchi, T. Sakurai, PNAS 101 (2004) 9966.
[137] T. Someya, Y. Kato, T. Sekitani, S. Iba, Y. Noguchi, Y. Murase, H. Hawaguchi, T. Sakurai, PNAS 102 (2005) 12321.
[138] T. Yamada, Y. Hayamizu, Y. Yamamoto, Y. Yomogida, A. Izadi-Najafabadi, D.N. Futaba, K. Hata, Nat. Nanotechnol. 6 (2011) 296.
[139] A.H.C. Koh, C.L. Ang, Ann. Acad. Med. Singapore 31 (3) (2002) 399.
[140] J.L. Stone, W.E. Barlow, M.S. Humayun, E. de Juan Jr., A.H. Milam, Arch. Ophthalmol. 110 (1992) 1634.
[141] A. Santos, M.S. Humayun, E. de Juan Jr., R.J. Greenburg, M.J. Marsh, I.B. Klock, A.H. Milam, Arch. Ophthalmol. 115 (1997) 511.
[142] S.Y. Kim, S. Sadda, J. Pearlman, M.S. Humayun, E. de Juan Jr., B.M. Melia, W.R. Green, Retina 22 (2002) 471.
[143] E. Zrenner, A. Stett, S. Weiss, R.B. Aramant, E. Guenther, K. Kohler, K.D. Miliczek, M.J. Seiler, H. Haemmerle, Vis. Res. 39 (1999) 2555.
[144] M. Humayun, R. Propst, E. de Juan Jr., K. McCornick, D. Hickingbotham, Arch. Ophthalmol. 112 (1994) 110.
[145] D. Palanker, A. Vankov, P. Huiel, S. Baccus, J. Neural Eng. 2 (2005) S105.
[146] S. Rajaraman, M.A. McClain, S.-O. Choi, J.D. Ross, S.P. DeWeerth, M.C. LaPlaca, M.G. Allen, in: Proc. 14th Int. Conf. Solid-State Sens., Actuators, Microsyst. (TRANSDUCERS), Lyon, France, 2007, p. 1252.
[147] R. Bhandari, S. Negi, L. Rieth, R.A. Normann, F. Solzbacher, in: Proc. 14th Int. Conf. Solid-State Sens., Actuators, Microsyst. (TRANSDUCERS), Lyon, France, 2007, p. 1231.
[148] K. Hungar, M. Görtz, E. Slavcheva, G. Spanier, C. Weidig, W. Mokwa, Sens. Actuators A 123 (2005) 172.
[149] A. Hung, D. Zhou, R. Greenberg, J.W. Judy, in: Proc. 2nd Int. IEEE EMBS Conf. Neural Eng., Arlington, VA, 2005, p. 179.
[150] E.T. Kim, J.-M. Seo, S.J. Woo, J.A. Zhou, H. Chung, S.J. Kim, Sensors 8 (2008) 5845.
[151] M.S. Humayun, J.D. Weiland, G.Y. Fuji, R. Greenberg, R. Williamson, J. Little, Vis. Res. 43 (2003) 2573.
[152] C. Veraat, M.C. Wanet-Defalque, B. Gerard, A. Vanlierde, J. Delbeke, Artif. Organs 27 (2003) 996.
[153] J.F. Rizzo III, J. Wyatt, J. Loewenstein, S. Kelly, D. Shire, Invest. Ophthamol. Vis. Sci. 44 (2003) 5355.
[154] L.-F. Chen, N. Hu, N. Liu, B. Guo, J. Yao, L. Xia, X. Zheng, W. Hou, Z.Q. Yin, Cell Tissue Res. 340 (2010) 421.
[155] Y. Sun, S.P. Lacour, R.A. Brooks, N. Rushton, J. Fawcett, R.E. Cameron, J. Biomed. Mater. Res. A 90A (2008) 648.
[156] E. Guenther, B. Troger, B. Scholosshauer, E. Zrenner, Vis. Res. 39 (1999) 3988.
[157] K.-I. Koo, S. Lee, S.H. Bae, J.M. Seo, H. Chung, D.-I. Cho, J. Microelectromech. Syst. 20 (2011) 251.

[158] P. Bergonzo, A. Bongrain, E. Scorsone, A. Bendali, L. Rousseau, G. Lissorgues, P. Mailley, Y. Li, T. Kauffmann, F. Goy, B. Yvert, J.A. Sahel, S. Picaud, IRBM 32 (2011) 91.
[159] M. Kopecek, et al., Phys. Status Solidi (A) Appl. Mater. 205 (2008) 2146.
[160] R. Roblee, Neural Prostheses — Fundamental Studies, Prentice Hall, 1990.
[161] L.M. Sanders, J.S. Kent, G.I. McRac, B.h. Vickery, T.R. Tice, D.H. Lewis, J. Pharm. Sci. 73 (1984) 1294.
[162] H. Okada, M. Yamamoto, T. Heya, Y. Inoue, S. Kamei, Y. Ogawa, H. Toguchi, J. Control. Release 28 (1994) 121.
[163] E. Jo, S. Lee, K.T. Kim, Y.S. Won, H.S. Kim, E.C. Cho, U. Jeong, Adv. Mater. 21 (2009) 968.
[164] H.S. Hu, Y. Chen, D.M. Liu, C.S. Hsiao, Adv. Mater. 20 (2008) 2690.
[165] M.J. Tiemey, C.R. Martin, J. Electrochem. Soc. 137 (1990) 3789.
[166] J.T. Santini, M.J. Cima, R. Langer, Nature 397 (1999) 335.
[167] E.R. Edelman, J. Kost, H. Bobeck, R. Langer, J. Biomed. Mater. Res. 19 (1985) 67.
[168] J. Kost, J. Wolfrum, R. Langer, J. Biomed. Mater. Res. 21 (1987) 1367.
[169] L.E. Bromberg, E.S. Ron, Adv. Drug Delivery Rev. 31 (1998) 197.
[170] D. Needham, M.W. Dewhirst, Adv. Drug Delivery Rev. 53 (2001) 285.
[171] O.V. Gerasimov, J.A. Boomer, M.M. Qualls, D.H. Thomson, Adv. Drug Delivery Rev. 38 (1999) 317.
[172] D.C. Hyun, G.D. Moon, C.J. Park, B.S. Kim, Y. Xia, U. Jeong, Angew. Chem. Int. Ed. 50 (2011) 724.
[173] K. Tsioris, W.K. Raja, E.M. Pritchard, B. Panilaitis, D.L. Kaplan, F.G. Omenetto, Adv. Funct. Mater. 22 (2012) 330.
[174] S. Sullivan, N. Murthy, M. Prausnitz, Adv. Mater. 20 (2008) 933.
[175] S. Davis, B. Landis, Z. Adams, M. Allen, M. Prausnitz, J. Biomech. 37 (2004) 1155.
[176] G. Altman, F. Diaz, C. Jakuba, T. Calabro, R. Horan, J. Chen, H. Lu, J. Richmond, D. Kaplan, Biomaterials 24 (2003) 401.
[177] C. Jiang, X. Wang, R. Gunawidjaja, Y. Lin, M. Gupta, D. Kaplan, R. Naik, V. Tsukruk, Adv. Funct. Mater. 17 (2007) 2229.
[178] E.M. Aliot, W.G. Stevenson, J.M. Almendral-Garrote, F. Bogun, C.H. Calkins, E. Delacretaz, P.D. Bella, G. Hindricks, P. Jaïs, M.E. Josephson, J. Kautzner, G.N. Kay, K.H. Kuck, B.B. Lerman, F. Marchlinski, V. Reddy, M.J. Schalij, R. Schilling, K. Soejima, D. Wilber, Europace 11 (2009) 771.
[179] B.J. Scherlag, S.H. Lau, R.H. Helfant, W.D. Berkowitz, E. Stein, A.N. Damato, Circulation 39 (1969) 13.
[180] J. Viventi, D.-H. Kim, J.D. Moss, Y.S. Kim, J.A. Blanco, N. Annetta, A. Hicks, J. Xiao, Y. Huang, D.J. Callans, J.A. Rogers, Sci. Transl. Med. 2 (24) (2010).
[181] D.-H. Kim, J. Viventi, J.J. Amsden, J. Xiao, L. Vigeland, Y.-S. Kim, J.A. Blanco, B. Panilaitis, E.S. Frechette, D. Contreras, D.L. Kaplan, F.G. Omenetto, Y. Huang, K.-C. Hwang, M.R. Zakin, B. Litt, J.A. Rogers, Nat. Mater. 9 (2010) 511.
[182] D.-H. Kim, N. Lu, R. Ma, Y.S. Kim, R.-H. Kim, S. Wang, J. Wu, S.M. Won, H. Tao, A. Islam, K.J. Yu, T.-I. Kim, R. Chowdhury, M. Ying, L. Xu, M. Li, H.-J. Chung, H. Keum, M. McCormick, P. Liu, Y.-W. Zhang, F.G. Omenetto, Y. Huang, T. Coleman, J.A. Rogers, Science 333 (2011) 838.